Selective Transport of NH_3 by Silica-Based Ceramic Pervaporation Membrane

Yundan Wang

Delft University of Technology

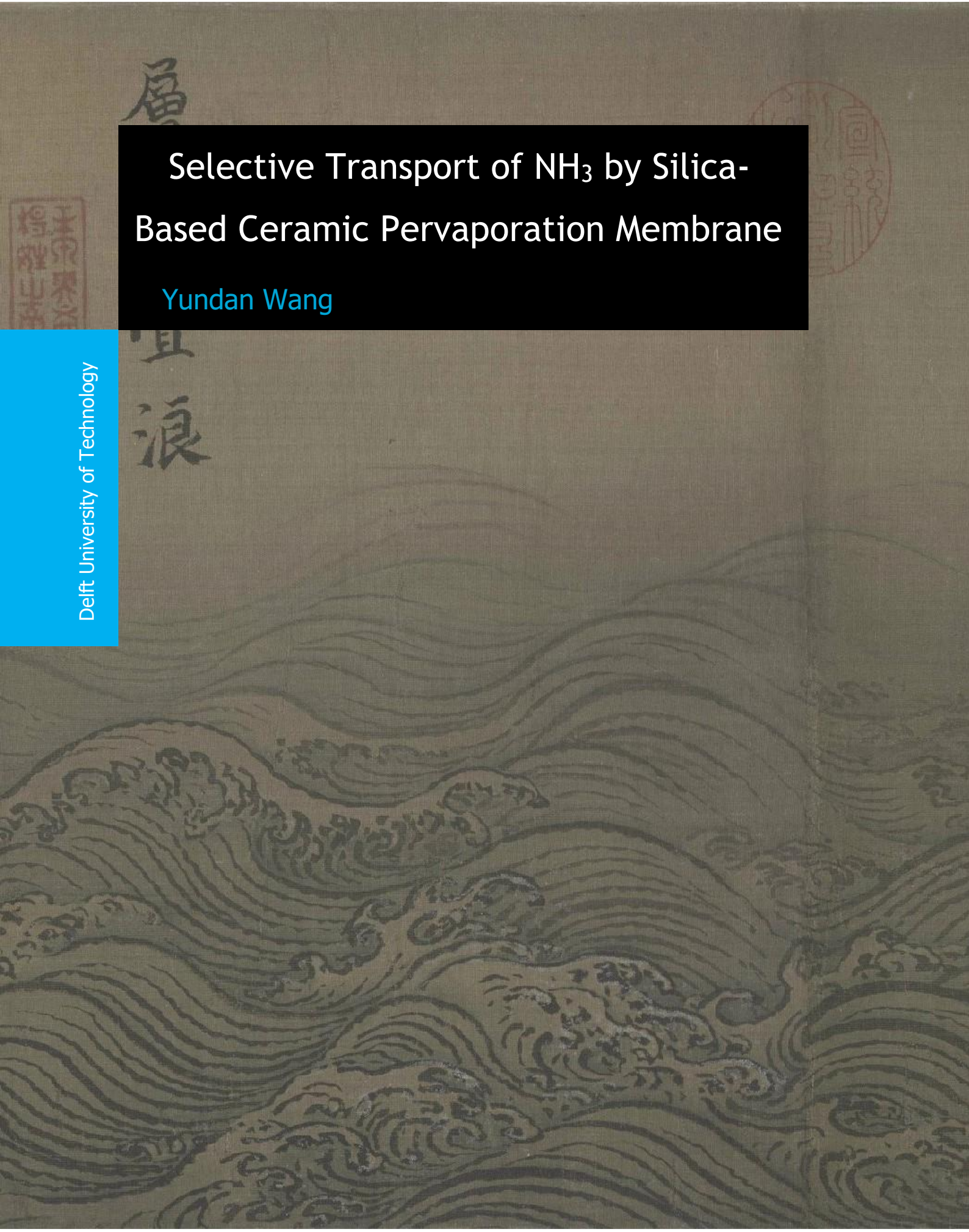

TU Delft Delft University of Technology

Challenge the future

Selective Transport of NH_3 by Silica-Based Ceramic Pervaporation Membrane

By

Yundan Wang

For the degree of

Master of Science in Civil Engineering

Supervisor:	Ir. Niels van Linden	TU Delft
Thesis committee:	Prof. Dr. Ir. Jules van Lier	TU Delft
	Dr. Ir. Henri Spanjers	TU Delft
	Dr. Ir. Ran Shang	TU Delft
	Dr. Xuerui Wang	TU Delft

Thursday, 31th January 2019

TU Delft Delft University of Technology

Acknowledgements

Seven years ago, almost reluctantly, I started my bachelor entitled Water and Wastewater Since and Engineering. I had tried to pursue my initial interest but failed. Fortunately, a growing interest was built later on as I grasping more insights of this subject, but simultaneously came along with responsibility. Gradually, I realized that environmental issues are more about environmental awareness, which triggered me to go abroad to see how these issues are treated worldwide.

Up till the end of the first year of my MSc, I was still an amateur of research. To tickle my curiosity, I decided to spend the rest of the MSc on pure research: water research course, additional thesis and final MSc thesis. A very brave decision I would say now since research never went as expected and things were only known afterwards. Motivated, frustrated, exhausted, inspired and anxious came to me quite often especially when my membrane turning pink and feed solutions turning blue. But I am so glad and proud that at least one of them can be pinpointed now. What a brainstorm! Thanks to those outliers for making this journey more meaningful and making me more resilient.

However, it was impossible for me to accomplish my thesis without the help from many people. So, I would like to thank my daily supervisor, Ir. Niels van Linden, who is very supportive, patient and considerate and is always available for discussions, questions and instructions. Thank you for getting me back on track in time when I was trapped during the research. Discussion with you was very inspiring, through which I learned a lot. Thank you also for giving me the opportunity to join the group reporting for part of the ZERO BRINE project.

In addition, I would like to thank Dr. Ir. Henri Spanjers, for your support during both my additional thesis and MSc thesis. Most gratefully, thank you for introducing the "N2kWh-From pollutant to power" project and the technology of pervaporation to me at the time when I was seeking for an MSc thesis topic. If not, nothing afterwards would be possible. I would like to thank Dr. Ir. Ran Shang, especially for your guidance during the water research course, which was very valuable for my following MSc thesis. I also would like to thank other members of my graduation committee, Prof. Dr. Ir. Jules van Lier, and Dr. Xuerui Wang for your critical comments during meetings. Furthermore, I would like to thank Prof. Ernst Sudhölter for joining the discussions since my greenlight meeting and for sharing very insightful and appealing ideas.

Besides, I would like to thank study advisor, Pascal de Smidt, for your very helpful advice on my study programme. Also, thanks to the staff in the Waterlab: Armand Middeldorp, Mohammed Jafar and Patricia van den Bos for making experiments a little bit easier.

Two and a half years here in the Netherlands broadens my horizon, visually and mentally. It really was not easy at the beginning but turns out to be very valuable and memorable. So, I would like to thank my old friends for tolerating my waffling and for sharing joy and sorrow in life. Thanks to my new friends for bringing lots of fun. Thanks to the Dutch winter weather, windy, cloudy and rainy, for stopping me going out but to study under roof. Finally, I would like to thank my parents for everything except occasionally disturbing me with only photos of hometown food. Thanks to my grandparents for being in good health, which I care about the most every time I go for a long journey.

Yundan Wang,

Delft, January 2019

Abstract

Nitrogen (N) removal is one of the key tasks for every wastewater treatment plant under the growing pressure of environmental protection. Prevailing applied N treatment technologies are mostly energy-intensive. This dilemma triggers a rethinking of the way to approach N management. "N2kWh-From pollutant to power" is a project that aims at creating an energy-positive N treatment system by exploiting the energy potential stored in reduced N compounds. Both thermal and electrical energy needed in this scheme will be provided by Solid Oxide Fuel Cell (SOFC) using the ammonia recovered from wastewater. To guarantee a proper function of the SOFC a minimum of 5 wt% of ammonia in the gas mixture is a prerequisite, whereas, the reject water of anaerobic digester only typically contains 0.15 wt%. Therefore, selectively stripping NH_3 in waste streams is the main technical bottleneck of this project.

This study aims at contributing to the understanding of selective transport of NH_3 by pervaporation. A comprehensive literature study indicates silica-based ceramic membrane is able to perform this selective transport. Therefore, the task of this research was to test the feasibility of selective transport of NH_3 by commercially available silica-based pervaporation membranes (hydrophobic PDMS and hydrophilic Hybrid Si AR). The objective was to find the optimum operating condition for maximizing the selective transport of NH_3 by silica-based ceramic pervaporation membrane. To this end, the impact of flow regime (laminar and turbulent flow), temperature (35 °C and 45 °C), presence of additional salt ($NaCl$ and Na_2CO_3) and TAN concentrations (total ammonium nitrogen; 1.5, 12.0 and 20.0 g TAN·L^{-1}, respectively) was assessed through a series of systematic experiments.

It was found that the PDMS membrane was unable to selectively transport NH_3 from liquid solution because both H_2O and NH_3 are polar molecules while the hydrophobic PDMS was nonpolar. Besides, the PDMS membrane tested was not stable under solutions used in this study.

The results of Hybrid Si pervaporation membrane showed that the optimum operating conditions for selective transport of NH_3 was 35 °C, Re=2,400, 20.0 g TAN·L^{-1} ammonium bicarbonate solution (pH adjusted to 10). For these conditions, the highest perm-selectivity (ratio of mass transfer coefficients of NH_3 and H_2O) was 0.5 indicting NH_3 was less selectively transported than H_2O.

The impact of flow regime on selective transport of NH_3 was related to polarization effects and depended on TAN concentration in feed solution. In the tested temperature and TAN concentration range, perm-selectivity was independent on both parameters. In addition, the effect of both temperature and TAN concentration on the ammonia was mainly due to the driving force, so their influence on the perm-selectivity was limited. Presence of salt seemed to have a positive impact on the perm-selectivity. Although salt has little impact on the mass transfer coefficient of NH_3, it decreased the mass transfer of H_2O resulting in a better selective transport of NH_3.

As for energy consumption, it was inversely related to TAN content. At the optimum operating condition 7 MJ·kg^{-1} - N was consumed by pervaporation in this study. Compared with the energy consumption of air stripping, pervaporation is a promising technology for N recovery.

Table of Content

Abbreviations

Amm	Ammonia
Amm+	Ammonium
AmmBiC	Ammonium Bicarbonate
AmmOH	Ammonium Hydroxide
DCMD	Direct Contact Membrane Distillation
Demi-water	Demineralised Water
EC	Electrical Conductivity
LHV	Lower Heating Value
MD	Membrane Distillation
MTC	Mass Transfer Coefficient
PDMS	Poly Di Methyl Siloxane
PV	Pervaporation
RO	Reverse Osmosis
SOFC	Solid Oxide Fuel Cell
TAN	Total Ammonia Nitrogen
TIC	Total Inorganic Carbon
TN	Total Nitrogen
VMD	Vacuum Membrane Distillation
VOCs	Volatile Organic Carbons
WWTP	Wastewater Treatment Plant

Symbols List

Nomenclature

A	Effective membrane area, [m^2]
$[A], [B], [C], [D]$	Activities of species, [$mol \cdot L^{-1}$]
A_T, B_T	Temperature dependent parameters, [-]
a, b, c, d, e	Constants
a_i, b_i	Ion-specific fit parameters
a_i	Activity of i, [$mol \cdot L^{-1}$]
C_f	Concentration of permeable molecules in the feed bulk solution, [$g \cdot L^{-1}$]
C_f'	Concentration of impermeable molecule in the feed bulk solution, [$g \cdot L^{-1}$]
C_i	Concentration of permeable molecules at the feed-membrane interface, [$g \cdot L^{-1}$]
c_i	Concentration of ion i, [$mol \cdot L^{-1}$].
C_i'	Concentration of impermeable molecule at the feed-membrane interface, [$g \cdot L^{-1}$]
C_m	Concentration in the membrane layer, [$g \cdot L^{-1}$]
$c_{NH_{3,t_n}}$	NH_3 Concentration at t_n, [$kg \cdot L^{-1}$]
c_{gas}	Concentration of aimed gas in solution, [$kg \cdot m^{-3}$];
D	Diffusion coefficient), [$m^2 \cdot s^{-1}$]
D_L	Diffusion coefficient, [$m^2 \cdot s^{-1}$]
d_h	Hydraulic diameter of a membrane module, [m]
f_i	Fugacity of gas i, [Pa]
h_{ov}	Overall heat transfer coefficient, [$J \cdot m^{-2} \cdot h^{-1} \cdot K^{-1}$]
h_f	Heat transfer coefficient at the feed side, [$J \cdot m^{-2} \cdot h^{-1} \cdot K^{-1}$]
h_m	Heat transfer coefficient of the membrane layer, [$J \cdot m^{-2} \cdot h^{-1} \cdot K^{-1}$]
I	Ionic strength, [$mol \cdot L^{-1}$]
J	Flux, [$kg \cdot m^{-2} \cdot h^{-1}$]
K	Equilibrium constant, [-]
K°	Standard equilibrium constant, [-]
K_H	Henry's law constant, [$m^2 \cdot s^{-2}$]
k_{ov}	Overall mass transfer coefficient, [$s \cdot m^{-1}$] or [$m \cdot s^{-1}$] linked by Henry's law constant
k_f	Mass transfer coefficient at the feed side, [$m \cdot s^{-1}$]
k_m	Mass transfer coefficient of the membrane layer, [$m \cdot s^{-1}$]
L	Length of a membrane tube, [m]
m_{total,t_n}	Total mass at t_n, [kg]
Nu	Nusselt number, [-]
n_{total}	Sum of mole of each component in the gas mixture, [mole]
P	Partial pressure, [Pa]
P_{gas}	Partial pressure of aimed gas, [Pa]
P_i^*	Saturated vapor pressure of i, [Pa]
p	Permeability, [$m^2 \cdot s^{-1}$]

Pr	Prandtl number, [-]
Q	Overall heat flux, [J·m^{-2}·h^{-1}];
R	Universal gas constant, 8.314 [J·mol^{-1}·K^{-1}]
Re	Reynolds number, [-]
R_{ov}	Overall resistance, [s·m^{-1}]
R_f	Resistance at the feed side, [s·m^{-1}]
R_m	Resistance of the membrane layer, [s·m^{-1}]
R_p	Resistance at the permeate side, [s·m^{-1}]
S	Solubility coefficient, [-]
Sh	Sherwood number, [-]
Sc	Schmidt number, [-]
T	Temperature, [°C] or [K]
T°	Temperature at standard condition, 298.15 [K];
T_f	Temperature of the feed bulk solution, [°C]
T_i	Temperature at the feed-membrane interface, [°C]
T_m	Temperature at the membrane layer, [°C]
V	Volume of the gas mixture, [m^3]
V_{t_n}	Total volume of feed solution at t_n [L]
z_i	Electric charge of ion i, [-]
$\Delta_r G^\circ$	Standard Gibbs Free Energy, [kJ·mol^{-1}]
$\Delta_r H^\circ$	Standard enthalpy of a reaction, [kJ·mol^{-1}]
$\Delta H_{vap,\,NH_3}$	Enthalpy change of NH_3, [kJ·mol^{-1}]
$\Delta H_{vap,\,H_2O}$	Enthalpy change of H_2O, [kJ·mol^{-1}]
$\Delta H'_{NH_{3-N}}$	Consumed thermal energy by pervaporation of NH_3, [MJ·kg^{-1} -N]
Δm_i	Mass difference, [kg]
Δt	Time slot, [h]

Subscripts

f	Membrane feed side
p	Membrane permeate side

Greek symbols

α	Perm-selectivity, [-]
β	Concentration factor, [-]
γ_i	Activity coefficient
υ	Flow velocity, [m·s^{-1}]
ν	Kinematic viscosity, [m^2·s^{-1}]
μ	Dynamic viscosity, [kg·m^{-1}·s^{-1}]
ρ	Density, [kg·m^{-3}]
λ	Heat conductivity, [J·m^{-1}·K^{-1}]
χ_i	Mole fraction of i, [-]
$\varphi_{i,(T)}$	Fugacity coefficient of i at temperature T, [-]

1 Introduction

1.1 Background

Nitrogen (N), a vital resource for industry and agriculture, plays an important role in modern civilization. After being processed and being consumed or digested (Figure 1), N is usually present in the form of organic and inorganic compounds in waste streams. Discharge of these streams causes serious environmental issues such as eutrophication. In the Netherlands, the regulation on the discharge of effluent regarding TN (total nitrogen) is 10 mg $N \cdot L^{-1}$ (Rijkswaterstaat, 2018). Controlling the effluent nitrogen level has become one of the crucial tasks of every wastewater treatment plant (WWTP).

The current state-of-art technologies for N removal from waste streams are biology-based nitrification and denitrification processes. By means of that, N is converted into nitrogen gas (N_2) and is eventually released into the atmosphere at a high energy cost. Guerrini, et al. (2017) shows that 41 $MJ \cdot kg^{-1}$-N energy is required to remove N from domestic wastewater. Within the N treatment processes, aeration, being the most energy-intensive step, accounts for up to 70% of the overall energy expenditure of a conventional WWTP (Beck et al., 2006; EDI, 2011; Rosso et al., 2008). Although this step is governing the energy efficiency of the entire treatment process, it is indispensable because nitrification needs it. This fact triggers an increasing demand for a new N removal method that is more energy-efficient.

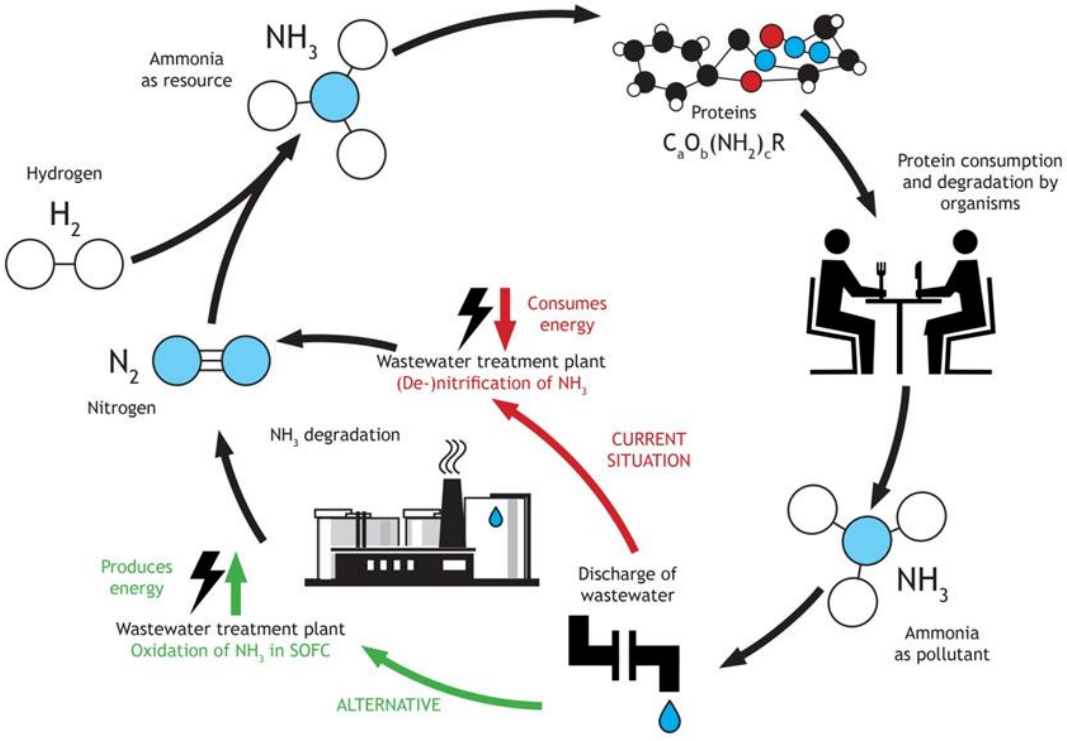

Figure 1 Ammonia cycle: from production to prevention of environmental pollution

Ammonia (NH_3), the primary inorganic nitrogen compound in wastewater, is a potential green energy carrier (Valera-Medina et al., 2018). On the one hand, the hydrogen mass fraction of NH_3 is 18 wt%, which is comparable to that of methane (25 wt%), highlighting the commercial potential of NH_3 as a fuel. A gross estimation shows that 14 MJ·kg^{-1}-N (based on LHV) of energy can be produced using solid oxide fuel cell (SOFC) (Dekker et al, 2006). Considering this fact, it is expected that the energy input for N removal can be reduced by recovering N in the wastewater as NH_3 that is further processed in an SOFC to produce enough energy to compensate for the energy consumed in the N removal. On the other hand, using NH_3 as an energy resource results in no CO_2 emission making NH_3 more environmental-friendly and sustainable than other carbon-based fuels. Nevertheless, the validity of NH_3 as an energy source has not been identified yet so far in the field of wastewater management.

1.2 N2kWh-From pollutant to power

"N2kWh-From pollutant to power" is an energy-oriented project that aims at narrowing down the energy imbalance of N removal by addressing the value of NH_3 in wastewater streams. The novel idea of this project is to develop a new combined system that integrates N removal and energy generation. In this scheme, N is removed by recovery as NH_3, and the total energy of the whole scheme would be provided by SOFCs fueled with NH_3 recovered so that no demanding of external energy input anymore. The ultimate goal of "N2kWh-From pollutant to power" project is to lead a paradigm shift of traditional wastewater management, in which pollutants are no longer treated as wastes but valuable resources instead.

In general, this project consists of two research tracks covering organic and inorganic types of N. One of them focuses on the stream that contains high carbon concentration and high nitrogen concentration (i.e., organic waste streams. The other focuses on the stream with high nitrogen content but with low carbon (i.e., inorganic waste streams). Three core research tasks are defined for the latter track. They are: firstly, to concentrate and produce gaseous NH_3; secondly, to evaluate SOFC performance on the produced NH_3 fuel; and the last, to customize pre-treatment processes for different waste streams. This research focusing on the NH_3 concentration by means of pervaporation belongs to task one.

One typical inorganic N-concentrated waste stream is rejected water from the digester in a typical WWTP. It is the internal liquid flow resulting from dewatering of anaerobically digested sludge containing about 20% of the total N load of a WWTP (Thorndahl, 1993). In this flow, N presents mainly as ammonium bicarbonate (NH_4HCO_3) in an approximate concentration of 1.5 g TAN·L^{-1} (TAN, total ammonia nitrogen defined as the sum of ammonia and ammonium). Due to this relatively high N concentration, reject water is considered more feasible for recovering N than municipal wastewater.

1.3 Problem Description

The power generator considered in the "N2kWh-From pollutant to power" project is an SOFC, which is an energy conversion technology that transfers chemical energy of a fed fuel directly into electrical and thermal energy through electrodes and electrolyte (Stambouli et al., 2002). The electrical efficiency of an ammonia-fueled SOFC is about 75% and can increase to 90% if thermal energy is recovered simultaneously (Guerrini et al., 2017; Stambouli et al, 2002). Due to this high energy conversion efficiency SOFC is considered to be more promising for power generation than other power generators, like internal combustion (IC) engine (the energy efficiency of which is 40% when using NH_3) (Giddey et al., 2017).

In an SOFC system, electrodes and electrolyte are integrated into a solid ceramic membrane where chemical reactions take place at membrane two sides separately under high temperature (700 °C) (Stambouli et al., 2002). Figure 2 depicts the working principle of SOFC: reduction of oxygen occurs at the cathode side where oxygen molecules receive electrons and mobilize to the anode side; at this side, at temperature around 700 °C, gaseous NH_3 is cracked into nitrogen gas (N_2) and hydrogen gas (H_2); subsequently, H_2 is oxidized forming water (H_2O) with reduced oxygen (O^{2-}) and releasing heat spontaneously. In return, electrons migrate to cathode side bridging the two half-reactions. It is because of the current formed by the moving electrons that electricity is produced. Specifically, the material that is coated on the anode layer of the SOFC used in this project is doped with nickel (Ni), which presents a strong affinity towards NH_3 and plays as a catalyst to accelerate NH_3 cracking.

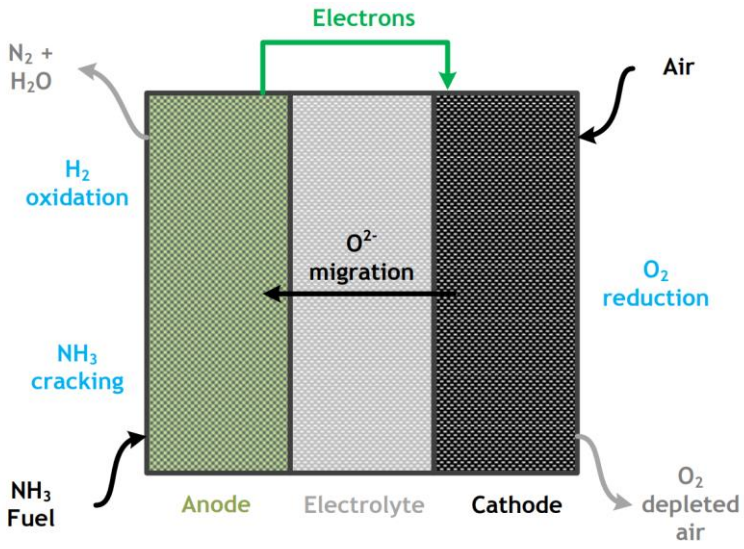

Figure 2 Schematic illustration of working principle of a SOFC.

The efficiency of SOFC depends on the quality of fed fuel. Good quality of fuel is a prerequisite to guarantee a proper functioning of a SOFC. However, up till now, little solid research about the impact of the composition of NH_3 fuel on the performance of SOFC have been published yet (van Linden et al., 2016). Desk research and internal experimental tests provide some quality and quantity requirements on the ammonia gas mixture to be supplied to SOFCs:

- Minimum 5 wt% of ammonia in the fed fuel

  Internal research shows 5 wt% is the bottom line for SOFC to function.

- Desiring an NH_3 content higher than 5 wt% giving three reasons:
  - Impurities are toxic for SOFC

    At the anode side, the Ni-coated fuel cell can be corroded by the presence of oxidants (Stambouli et al., 2002). According to Papadias et al. (2012), Ni can also react with H_2S to form NiS being out of function as a catalyst; besides, siloxanes, organic silicon compounds, is also a threat to the life expectancy of toxic. Because its presence in the fuel will lead to a formation of SiO_2 that can affect components in a SOFC system, such as sensors and heat exchangers.

  - A higher NH_3 content makes SOFC more energy-efficient

    Because, as aforementioned, SOFC performs at a rather high temperature, the fed fuel will present in a gaseous state inside the cell. However, the changing of phase from liquid to gas requires energy input. The part of the energy for changing the phase of ammonia is considered useful because it is inevitable in a way. But the part of the energy for changing the phase of other compositions like H_2O is useless and should be controlled by reducing its content in the fuel.

  - A higher NH_3 content is benificial for keeping a small footprint of a SOFC

    Supposing the flow rate is the same, to produce the same amount of energy at a given time, the SOFC system fed with NH_3-concentrated fuel can be more compact (smaller membrane area) than that fed with less NH_3-concentrated fuel and therefore is also more economical.

- A gaseous state is also desired. It is also for an energy-saving purpose, to reduce the energy input for phase change of fed fuel.

However, notably, the NH_3 content in the reject water is merely 0.15 wt% and with a lot of impurities. Hence one crucial breakthrough needs to be achieved within the "N2kWh-From pollutant to power" project is to recover NH_3 from the reject water that can be processed into SOFCs for efficient energy production (i.e. meet the above-mentioned requirements). Pervaporation (PV) is then proposed as a possible solution due to its ability of selective transport of species.

1.4 Pervaporation

1.4.1 State-of-the-art

Pervaporation refers to a process where species in the liquid phase firstly permeate through a membrane and ultimately evaporate into the vapour phase in the permeate side (Böddeker, 1990; Vane, 2005). Literally, mass transfer is achieved with the combination of 'permeate' and 'evaporate,' hence 'pervaporation.' The driving force for the mass transfer is the chemical potential gradient of the permeate established along the membrane thickness, which is usually the vapor pressure (Böddeker, 1990). Unlike reverse osmosis (RO), mass transfer of pervaporation is not restricted to the osmotic pressure, so the operating pressure is not necessarily high. Moreover, energy involved in pervaporation is for changing the phase of permeate (i.e. heat for vaporization) and alternatively for elevating the temperature of the feed solution (Ahmad et al., 2012), which makes the utility of low-grade heat source, like industrial waste heat, possible (Wang et al., 2016).

Membrane materials play an important role in the pervaporation process (See 2.1) (Jyoti et al., 2015; Shao et al., 2007; Wang et al., 2016). However, regarding its relatively small pore size, pervaporation membrane can hardly result in an economically satisfactory flux (Khayet et al., 2004; Park et al., 2017). The prosperity that enables pervaporation to be competitive to other separation technologies is the intrinsic affinity between membrane material and the target permeated species. This distinct attribute allows species that are dilute in the feed to be highly enriched in the permeate (i.e. selectively transported), which is difficult for technologies that utilize pure evaporation such as membrane distillation (Vane, 2005).

Membrane materials of pervaporation dictate the species that are selectively transported in the process. In general, pervaporation membrane can be categorized into two types. Those are hydrophilic pervaporation membrane and hydrophobic pervaporation membrane. The former exhibits affinity towards water over others (i.e. H_2O is selectively transported). Therefore, it is usually considered for the water purification purpose, for instance, desalination where water is preferentially allowed to pass through, while salts are retained (Wang et al., 2016). The latter, due to its hydrophobic nature, water is retained on purpose at the feed side and so enhancing the separation. Main industrial application of hydrophobic membrane is dehydration of organic solvents, especially those that form azeotropes with water, such as ethanol and isopropanol (Ahmad et al., 2012; Vane, 2005).

1.4.2 Selective Transport of Ammonia

However, comprehensive desk research (see 1.4) shows that a handful of studies in the field of pervaporation pay attention to NH_3 stripping from waste liquid solution; either few of them aims at NH_3 recovery (Camus et al., 2006; Hirabayashi, 2002; Yang et al., 2014, 2016). Precisely, no explicit clue can be pinpointed from the literature on what are optimum working conditions for NH_3 stripping via pervaporation (i.e. lack of understandings about the influence of operation parameters on selective transport of NH_3).

As for the selection of membrane material for NH_3 separation, the possibilities of both types of pervaporation membrane (hydrophilic and hydrophobic) have been estimated and reported by a few researchers among which the affinity between silica-based membrane and NH_3 has been announced occasionally.

An early study that applies pervaporation technology on NH_3 removal was conducted by Hirabayashi (2002), in which the performance of hydrophilic organic pervaporation membrane on water stripping from artificial urine

solution has been studied and proven to be feasible. In the article of this study, observation of Hirabayashi's previous research was mentioned that a type of hydrophobic membrane is able to selectively transport NH_3. However, report of this previous research is not publicly available. Thus no explicit indicating on how the investigation was conducted.

Camus et al. (2006) tested the behaviors of zeolite and hydrophilic silica pervaporation membranes on NH_3 recovery from a gas mixture (N_2, H_2, and NH_3) and showed that, for silica membrane, the permeance (ratio of the permeability to the thickness of a membrane) of NH_3 is higher than that of zeolite membrane whereas the corresponding perm-selectivity is lower.

Yang et al. (2014) achieved a permeate in which the NH_3 is about 60-fold more concentrated than that in the feed using customized hydrophilic pervaporation membrane at 50 °C being the best performance reported in the relevant literature so far. They attributed this highly selective transport of NH_3 to a combined transport mechanism of molecular diffusion and interactive ammonia-silica adsorption, peculiar to pervaporation membrane. Nevertheless, during a long-term experiment, a decay of total flux and unstable performance on selective transport of NH_3 of their pervaporation membrane was observed. According to their explanation, it was because of pore structure degradation. In their follow-up research, with improved membrane stability, the membrane was able to performed steadily regarding to NH_3 and H_2O permeance, but was unable to transport NH_3 as selectively as the pervaporation membrane tested before (Yang et al., 2016).

1.4.3 Effects of Operating Parameters

Flow Regime

When the flow regime of feed flow changes from laminar to transition by increasing the cross-flow velocity (i.e. Reynolds number), the mass transfer coefficient of H_2O is found to increase correspondently (Oliveira et al., 2001).

However, when the system is already in a fully turbulent flow regime, further increasing the cross-flow velocity is not energy-efficient. Because though the mass transfer continues to increase, energy consumption increases more significantly as a lot of energy is used for increasing the cross-flow velocity, but the improvement of mass transfer is limited. The positive impact of increasing the Reynolds number is associated with an improved boundary layer condition and as a consequence, reducing the mass transfer resistance in the liquid phase (Jiang et al., 1997; Oliveira et al., 2001). Yet, the impact of flow regime on NH_3 transport in the pervaporation process is basically unknown.

Temperature

Temperature being a key operation factor in pervaporation process has been extensively studied in pervaporation application on volatile organic carbons (VOCs). In general, increasing the temperature not only provides a higher driving force for mass transfer but also enhances the diffusivities of species inside the membrane structure, both of which lead to a higher mass flux (Peng et al., 2003; Wang et al., 2016). As for NH_3, Yang et al. (2014) who conducted experiments respectively at 25, 45 and 50 °C, claimed that, at 25 °C, the NH_3 adsorption to membrane matrix is more predominate than NH_3 desorption. Camus et al. (2006) declared that NH_3 diffusivity is positively related to temperature with a possible explanation that higher temperature increases the diffusion rate of NH_3 crossing the membrane structure. Yet, the validity of their results for liquid feed solutions has not been verified.

Nonetheless, with respect to permeate quality, there exists a dilution impact if species instead of H_2O are the

target compounds; because H_2O pressure increases exponentially as temperature increases meaning the extent of increase of driving force for H_2O is likely more significant than that of target species, like benzene (Peng et al., 2003). Thus far, the overall impact of temperature on each component in a binary ammonia-water feed solution is unclear especially the impact on factors like diffusion rate and so on.

Feed Concentration and Feed Composition

Feed concentration, to a large extent, affects the chemical potential gradient for mass transfer in the pervaporation process no matter in what form the potential is presented. When partial vapor pressure is adopted, the relation between feed concentration and partial vapor pressure is described by Henry's law and Raoul's law for solvent and solute respectively (see 2.4) (Jiang et al., 1997; Khayet et al., 2004). In general, increasing the concentration of one target species in the feed solution leads to a higher flux summarised in the review paper written by Peng et al. (2003).

On the contrary, an increased salt concentration in the feed solution has a negative impact on mass transfer with joint influence of various factors. Firstly, the driving force is directly affected although it has been theoretically proven to be limited. But the H_2O flux of a practical study showed a significant decrease by 30% when salt ($NaCl$) concentration increased from 0 to 100 mg L^{-1}, which might result from membrane fouling due to the presence of salt (Huth et al., 2014). Secondly, the diffusion coefficient of permeated molecules, species activities are impeded by increasing salt concentration in the feed liquid (Wang et al., 2016).

As for NH_3 stripping, Camus et al. (2006) discovered an inverse relationship between NH_3 concentration (ranging from 2 to 16 wt%) in the feed and the corresponding NH_3 permeance. They argued that the transporting of NH_3 is impeded as the saturated level increasing; and when membrane pores are saturated with NH_3 molecules, further increasing the feed concentration has no more significant impact due to a shift of governing mass transfer mechanism. However, again, this phenomenon was detected in a pervaporation system feed with a gas mixture.

1.5 Research Objective

This research aimed to contribute to the understanding of selective transport of NH_3 through pervaporation membranes in the context of "N2kWh-From pollutant to power" project. To this end, the research objective was:

"To find, the optimum operating condition for maximizing the selective transport of NH_3 by silica-based ceramic pervaporation membranes. "

The optimum operating condition was defined as the condition at which the perm-selectivity (α, defined as the ratio of permeabilities of permeated species; see 3.6.4 for details) was the highest. Membranes were selected according to the potential ability to selectively transport NH_3 suggested in the literature (see 1.4). Various combinations of temperature, feed concentration and flow regime were studied during the experiments in order to find the optimum condition (see 3.1).

1.6 Research Questions

To approach the objective two main research questions were formulated; the first one was addressed by explicit sub-questions; the second research question was proposed with emphasis to the energy consumption:

1. What is the optimum operating condition?
   a. What is the impact of flow regime on the flux, MTC and perm-selectivity?
   b. What is the impact of temperature on the flux, MTC and perm-selectivity?
   c. What is the impact of TAN concentration on the flux, MTC and perm-selectivity?
   d. What is the impact of additional salt on the flux, MTC and perm-selectivity?
2. How much energy is consumed per unit of permeated ammonia at the optimum operating condition?

1.7 Thesis layout

This thesis is structured into six sections as follows:

- Chapter 1 Introduction: Providing project background information and general problem description; state-of-the-art pervaporation especially focusing on selective transport of NH_3; ending up with specific research objective and research questions;
- Chapter 2 Theory: Containing working mechanisms of pervaporation with limitation discussed and associated fundamental physical-chemical theories;
- Chapter 3 Methods and Materials: Including the criteria of experimental conditions selection, experiment procedure together with related materials; analytical approaches followed by preliminary modelling results, general assumptions and hypothesis accordingly;
- Chapter 4 Results and Discussion: Presenting experimental results with in-depth analysis and discussion;
- Chapter 5 Conclusion: Summary of observations and answers to formulated research questions;
- Chapter 6 Recommendation: Proposing promising research topics for future study.

2 Theory

2.1 Mass transfer: Sorption-diffusion Mechanism

The sorption-diffusion mechanism is taken into account primarily when elucidating the performance of pervaporation (Khayet et al., 2004; Wijmans et al., 1995). It is the dominant mass transfer mechanism in the pervaporation process (Cheng et al., 2017). In this model, as depicted in Figure 3, transport occurs in three successive steps in corresponding layers:

1) Sorption: Molecules in the bulk solution are sorbed into the surface of a membrane;
2) Diffusion: Sorbed molecules diffuse through the membrane material following a chemical gradient which is usually the partial pressure;
3) Desorption: Molecules leave the membrane as a vapour permeate.

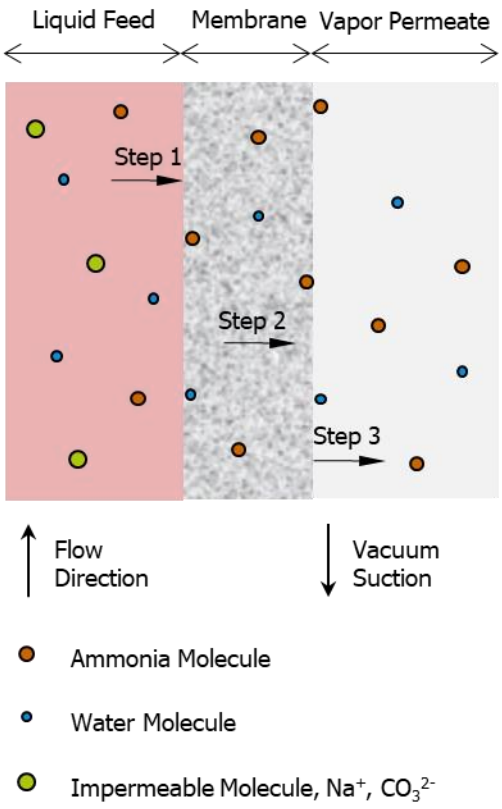

Figure 3 Demonstration of sorption-diffusion theory through a membrane profile: 1) molecules in the feed solution are selectively sorbed into the feed-membrane interface; 2) sorbed molecules diffuse within the membrane matrix driven by the partial pressure imposed over the membrane two sides; 3) desorption of molecules from the membrane and sucked away by a vacuum pump.

Accordingly, separation is achieved based on differences in sorption and the diffusion rates within the membrane matrix. This theory is established underlining two assumptions. Firstly, the whole pervaporation system is in a steady state: reactions (i.e., sorption, diffusion, and desorption) are in equilibrium. Secondly, no further component interactions exist except that between the target species and the membrane material (Khayet et al., 2004; Lipnizki et al., 2004). Referring to the sorption-diffusion model, assuming a uniform partial pressure gradient alongside the membrane thickness when vacuum is employed, the flux of a certain permeate can be formulated in terms of overall mass transfer coefficient:

$$J = k_{ov} \cdot (P_f - P_p) \cdot 3600 \qquad \textit{Eq. 1}$$

where

J – flux, [kg·m^{-2}·h^{-1}];

k_{ov} – overall mass transfer coefficient, [s·m^{-1}] since pressure was used here; Henry's law constant K_H can be used to convert the unit to [m·s^{-1}] (see 2.4.1);

P – partial pressure of species i, [Pa] or [kg·m^{-1}·s^{-2}];

with suffixes, f and p represent feed side and permeate side, respectively.

Within the sorption-diffusion theory, mass transfer is achieved as a result of the continuous movement of permeate through the three layers as shown in Figure 3. However, resistance ($R = \frac{1}{k}, k$ is the mass transfer coefficient) that is intrinsically existing in each layer acts against the movements of molecules. In the literature, the resistance-in-series-model is generally applied to describe the overall resistance, R_{ov}, shown in Eq. 2:

$$R_{ov} = R_f + R_m + R_p \qquad \textit{Eq. 2}$$

in which suffixes f, m and p refer to liquid feed layer, membrane layer and vapour permeate layer respectively.

In most cases, R_p is neglected due to applied vacuum pressure and so low concentration at the permeate side (Khayet et al., 2004; Wang et al., 2016). A more popular expression is substituting the resistance by the mass transfer coefficient (k) which yields:

$$\frac{1}{k_{ov}} = \frac{1}{k_f} + \frac{1}{k_m} \qquad \textit{Eq. 3}$$

In the literature, k_f and k_m are usually studied independently. Different theories are proposed for quantifying and are discussed in the following sections.

2.1.1 Mass Transfer Boundary Layer (Concentration Polarization)

According to the theory of fluid dynamics, at the liquid feed side, the resistance of the membrane surface results in a velocity profile established across the feed channel as depicted in Figure 4. In other words, the velocity decreases as the distance from the membrane surface decreases. Consequently, the flow at the feed-membrane interface is almost stagnant. But increasing the cross-flow velocity helps reducing the velocity gradient reducing the thickness of this stagnant layer. The flow regime associated with cross-flow velocity is closely linked to the concentration polarization effect in size-sieving membrane processes, like reverse osmosis (RO), where salt

concentrations in the permeate are lower than that in the feed. These retained salts form a concentration gradient throughout a region adjacent to the membrane feed side. This phenomenon can also be detected in any pervaporation processes no matter the selectively transported species is water or not (see Figure 5 b.). The layer, differentiating the properties of the bulk solution and that of the solution at the feed-membrane interface, is widely termed boundary layer. This layer usually grows until the system reaching a steady state when the amount entering in the boundary layer equals the amount leaving.

Instead of increasing the osmotic and operation pressure like RO, in pervaporation, compounds that are accumulated at the boundary layer directly influence the partial pressure of permeate at the feed side (see section 2.4) (Feng et al., 1997; Jiang et al., 1997).

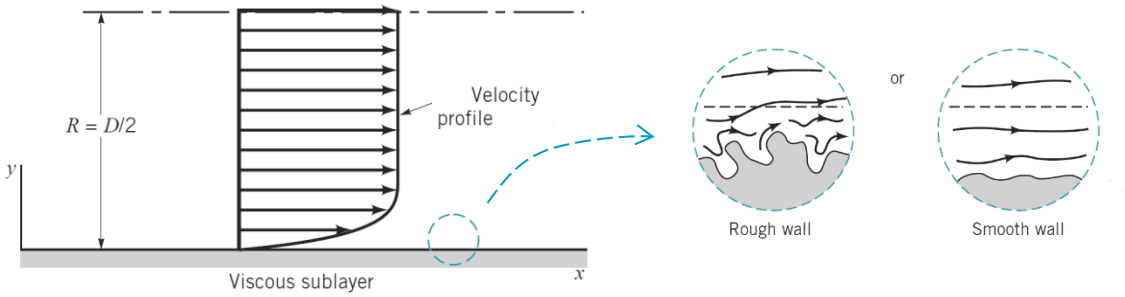

Figure 4 velocity profile of a tubular pipe flow. Adapted from (Munson et al., 2014).

Besides ions accumulation, for the pervaporation process, there is another type of concentration polarization originating from mass depletion (see Figure 5 a.). It is especially so when the target species are dilute in the feed solution. Because the compound is selectively transported, its concentration in the permeate is higher than that in the feed bulk solution. This concentration imbalance results in a descending trend of a concentration gradient of aimed species in the boundary layer as depicted in Figure 5 a. This depletion dilutes the aimed species reducing its driving force consequently. Moreover, this effect is particularly significant for highly selective applications (Wijmans et al., 1996; Zhang et al., 2016).

Concentration polarization leads to the fact that compounds that are enriched in the permeate are to be depleted in the boundary layer; and compounds that are depleted in the permeate are to be enriched in the boundary layer. Both aspects negatively influence the performance of the pervaporation membrane and should be avoided as much as possible. It has been proven that improving the hydraulic condition (i.e. flow regime) of the feed flow is beneficial for reducing the concentration gradient by creating a more evenly distributed solution (Wijmans et al., 1996).

In principle, to arrive at the permeate side, molecules need to first overcome the resistance of the boundary layer, R_f, which is commonly expressed by the mass transfer coefficient at the feed side, k_f. This coefficient is generally quantified using Sherwood number (Sh), which is a dimensionless number describing the concentration gradient at a surface and is formulated as the ratio of convective mass transfer rate (i.e., mass transfer parallel to the membrane surface) to the mass diffusion rate (i.e., mass transfer perpendicular to the membrane surface) (Bergman et al., 2011):

$$Sh = \frac{k_f d_h}{D_L} \qquad Eq.\ 4$$

where,

k_f – mass transfer coefficient at the feed side, [m·s^{-1}];

d_h – hydraulic diameter of a membrane module, [m];

D_L – diffusion coefficient of solute in a solvent, [m^2·s^{-1}].

In the literature, a common approach to calculate Sherwood number is applying Lévêque equation of which a general form is (Jyoti et al., 2015; Oliveira et al., 2001):

$$Sh = aRe^b Sc^c (\frac{d_h}{L})^e \qquad Eq.\ 5$$

with Reynolds number (ratio of the inertia and viscous forces)

$$Re = \frac{\upsilon \rho d_h}{\mu} = \frac{\upsilon d_h}{\nu} \qquad Eq.\ 6$$

and Schmidt number (ratio of the momentum and mass diffusivities)

$$Sc = \frac{\nu}{D_L} \qquad Eq.\ 7$$

where,

υ – flow velocity, [m·s^{-1}];

ν – kinematic viscosity, [m^2·s^{-1}];

μ – dynamic viscosity, [kg·m^{-1}·s^{-1}];

ρ – density of the solution, [kg·m^{-3}];

L – length of a membrane tube, [m];

a, b, c, e – empirical constants.

Constants in this semi-empirical Sherwood correlation depend on the geometry of a membrane module, the hydraulic condition applied and physical properties of the fluid and solution. Therefore they should be investigated specifically (Oliveira et al., 2001). With the different values of the exponents (b, c, e), the importance of convective mass transfer and mass diffusion are identified.

2.1.2 Mass Transfer Membrane Layer

The mechanism of mass transfer inside a membrane structure depends on the pore size. In the case of a membrane with a certain pore size distribution, kinds of mechanisms can contribute simultaneously but to different extents (Khayet et al., 2004). Considering the relatively small pore size of pervaporation membrane, mass transfer inside the membrane matrix is primarily characterized by "affinity" in accordance with the sorption-diffusion theory (Jyoti et al., 2015; Khayet et al., 2004; Lipnizki et al., 1999). Accordingly, estimation of membrane mass transfer

coefficient (k_m) is based on Eq. 8:

$$k_m = \frac{p}{\delta} \qquad \textit{Eq. 8}$$

with permeability, p in [$m^2 \cdot s^{-1}$]:

$$p = S \cdot D \qquad \textit{Eq. 9}$$

in which,

δ – membrane thickness, [m];

S – solubility (i.e. solubility coefficient), [-];

D – diffusivity (i.e. diffusion coefficient), [$m^2 \cdot s^{-1}$].

The solubility of a gas is usually described by Henry's law. The diffusivity of a penetrant depends on its geometry (i.e. molecular size), its concentration and the microstructure of membrane material, like tortuosity. A free volume theory is becoming more accepted to describe the behaviour of vapour molecules inside a membrane material (Cheng et al., 2017; Jyoti et al., 2015). Additionally, both solubility and diffusivity are partly depending on temperature: sorption is usually exothermic; whereas diffusion is proportionally related to temperature according to Stokes-Einstein equation (Frank et al., 1996; Jyoti et al., 2015). Hence, the overall impact of temperature on k_m is usually system-specific. As for the ammonia-silica system, this impact is unknown due to the lack of knowledge of the solubility and the diffusivity of NH_3 in the silica structure as a pervaporation membrane material.

Briefly, the dependence of k_m on temperature emphasizes the importance of heat transfer involved in pervaporation process of which theory is presented in section 2.2.

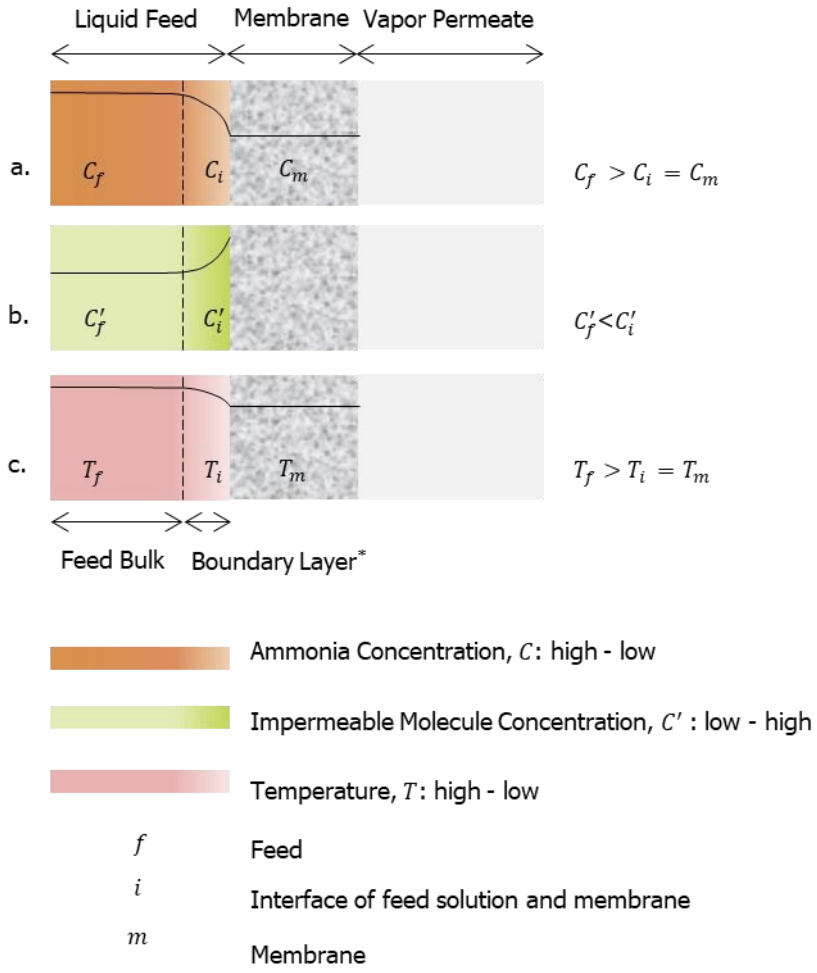

*Figure 5 Polarization Effects: a) concentration polarization due to mass depletion; b) concentration polarization due to mass accumulation; c) temperature polarization. *These concentration and temperature gradients are overlapped to a certain extent, but their thicknesses are not necessarily equal (Munson et al., 2014).*

2.2 Heat Transfer

2.2.1 Heat Consumption

Heat participates extensively in the pervaporation separation process. Steps that involve heat transfer are (Karlsson et al., 1996):

1) Sorption of molecules into the feed-membrane interface, $Q_{sorption}$;
2) The phase change of permeate from liquid to vapour, $Q_{evaporation}$;
3) Conduction: heat expansion within the membrane material and among vapour molecules due to direct contact, $Q_{conduction}$;
4) Desorption of vapour molecules from the membrane to the gaseous permeate side, $Q_{desorption}$.

Thus, the total heat consumed by pervaporation ($Q_{consumed}$) can be formulated into one equation:

$$Q_{consumed} = Q_{sorption} + Q_{evaporation} + Q_{conduction} + Q_{desoption} \qquad Eq.\ 10$$

Because sorption together with its reverse step desorption requires or releases the same amount of heat, the sum of $Q_{sorption}$ and $Q_{desorption}$ is theoretically equal zero (Favre, 2003; Karlsson et al., 1996). As for the heat transfer caused by conduction, it is considered negligible because it was assumed that there was no temperature gradient within the membrane matrix, as depicted in Figure 5 c (El-Bourawi et al., 2006). In addition, at the permeate side where vacuum pressure is applied, permeate is presenting in gaseous state and. Consequenctly, the overall heat consumption in particular for the pervaporation system used in this research can be written as:

$$Q_{concumed} = Q_{evaporation} \qquad Eq.\ 11$$

The portion of the heat required to change the phase is well-known as the latent heat which is quantified by the change of enthalpy (also termed the heat of vaporization) ΔH_{vap}.

2.2.2 Heat Transfer Boundary layer (Temperature Polarization)

Like mass transfer, the overall heat flux is described in terms of temperature difference:

$$Q = h_{ov}(T_f - T_p) \qquad Eq.\ 12$$

where

Q – overall heat flux, [J·m^{-2}·h^{-1}];

h_{ov} – overall heat transfer coefficient, [J·m^{-2}·h^{-1}·K^{-1}];

T – temperature, [K];

with suffix f and p stand for feed side and permeate side, respectively.

The resistance-in-series model is also applicable for heat transfer (Karlsson et al., 1996; Lawson et al., 1997):

$$\frac{1}{h_{ov}} = \frac{1}{h_f} + \frac{1}{h_m} \qquad \textit{Eq. 13}$$

Where the suffixes, ov, f and m represent to overall, membrane feed side and membrane layer, respectively.

In the boundary layer, due to the relatively low cross-flow velocity there, heat carried along with mass flow perpendicular to the membrane surface is more significant. In other words, flow rate near the feed-membrane interface is not rapid enough to compensate the heat loss due to mass transfer. The result is that a temperature gradient ($T_f > T_m$) develops at the boundary layer as shown in Figure 5 c. This phenomenon is commonly known as temperature polarization and can be commonly recognised in thermal-driven separation processes like pervaporation, membrane distillation (Favre, 2003; Lawson & Lloyd, 1997).

The most adverse influence of temperature polarization effect in pervaporation is on the driving force of permeate, which can lead to a less attainable flux. Moreover, because of the existence of temperature polarization, the liquid boundary layer where the major heat resistance locates dominates the overall heat transfer process (Favre, 2003). The same as concentration polarization, temperature polarization can be diminished to a certain degree by creating more turbulence in the feed flow. Favre (2003) claimed that a quasi-isothermal situation could be possibility reached when imposing highly turbulent flow.

As what Sherwood number is to mass transfer Nusselt Number (Nu, definded as the ratio of convection to pure conduction heat transfer) is to heat transfer (Karlsson et al., 1996; Martin, 2002). Its relation to heat transfer coefficient is:

$$Nu = \frac{h_f d_h}{\lambda} \qquad \textit{Eq. 14}$$

in which

h_f – boundary layer heat transfer coefficient, [J·m^{-2}·K^{-1}];

λ – heat conductivity, [J·m^{-1}·K^{-1}].

The Lévêque equation for Nusselt number can be acquired by substituting Schmidt number (Sc) with Prandtl Number (Pr, defined as the ratio of momentum and thermal diffusivities):

$$Nu = aRe^b Pr^c (\frac{d_h}{L})^e \qquad \textit{Eq. 15}$$

where

a, b, c, e – empirical constants.

Several semi-empirical correlations have been established regarding these constants for different membrane geometries under various flow regimes (Karlsson et al., 1996).

2.3 Limitation of Sherwood and Nusselt correlations

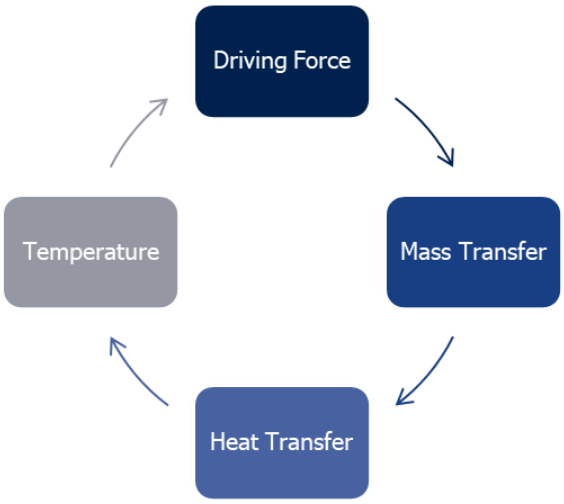

Figure 6 Intercorrelation between mass transfer and heat transfer linked by temperature in the pervaporation process.

As stated before, since pervaporation achieves gas extraction via phase changing, mass transfer is intrinsically correlated with temperature which is theoretically described by heat transfer. The relationship between mass transfer and heat transfer is illustrated in Figure 6 as a feedback loop:

- A partial pressure difference at the membrane two sides drives molecules to transport through (i.e. mass transfer) leading to an inevitable heat loss (i.e., heat transfer);
- Temperature drop being the consequence of heat transfer negatively reduces the driving force;
- Reduced driving force limits the mass transfer (i.e. decreases mass flux).

Apart from the driving force, properties of solution (such as viscosity, density, and diffusion coefficient) and molecule diffusion within membrane matrix are also temperature-related making the analysis of one pervaporation process more complicated. Briefly, mass and heat transfer are equally important in the pervaporation gas stripping process.

However, it is noteworthy that neither Sherwood correlations nor Nusselt correlations are able to elaborate this loop system in pervaporation process considering two aspects:

- Sherwood correlations lack the part of heat transfer and Nusselt correlations lack the part of mass transfer. Additionally, this limitation of Sherwood and Nusselt correlations can also be found in membrane distillation literature et al., 1997; Martínez-Díez et al., 1999). Therefore, both should be modified (Ito et al., 1997; Karlsson et al., 1996; Rautenbach et al., 1980). Favre et al. (2003) suggested a combined study of heat transfer and mass transfer.
- Sherwood correlations, being a method to estimate k_f, do not explicitly describe the concentration polarization effect which is important for the mass transfer in the boundary layer. The same for Nusselt correlations in which temperature polarization is not emphasized.

Despite so, the revealed incompleteness of Sherwood and Nusselt correlations has not been strategically

estimated yet in the field of pervaporation.

Besides, although the interaction between membrane material and permeate species is stressed in the sorption-diffusion theory, research on the interaction particularly between hybrid silica and NH_3 (i.e., the solubility of NH_3 gas in silica structured PV membrane) is scarce. In other words, the specific affinity between silica and NH_3 has not been fully understood yet.

Due to the knowledge gaps mentioned above, an attempt of an in-depth study of the mass transfer coefficients of the boundary layer and the membrane layer had been withdrawn in this study. Further study could target at these knowledge gaps for a more comprehensive understanding of the pervaporation process.

More detailed discussion on the limitation of Lévêque approach for mass and heat transfer can be found in the article reported by Karlsson et al. (1996) and the book written by Rautenbach et al. (1980). Limitations relevant with sorption-diffusion mechanism revealed by Heintz et al. (1994) and Krishna et al. (1997) can also be found in the literature.

2.4 Partial Pressure

2.4.1 Feed Side - Henry's Law & Raoul's Law

Henry's Law

Henry's Law is applied for ideal dilute solution (in which solvent strictly follows Raoult's Law and solute strictly follows Henry's Law) to describe the relationship between the concentration of dissolved gas and its partial pressure above the solution as formulated in Eq. 16 (Lide et al., 2009; Nivaldo, 2014):

$$P_{gas} = K_H \cdot c_{gas} \qquad Eq.\ 16$$

In which,

P_{gas} – partial pressure of aimed gas, [Pa] or [kg·m^{-1}·s^{-2}];

c_{gas}- concentration of aimed gas in solution, [kg·m^{-3}];

K_H – Henry's law constant, [m^2·s^{-2}].

The Henry's law constant is a specific parameter for a given gas, solvent and temperature as well; and its unit varies with the unit used for pressure and concentration (Nivaldo, 2014).

In this study, the partial pressure of NH_3 at the membrane feed side can be illustrated using Henry's Law. It simply indicates that when the temperature is fixed the partial pressure of NH_3 is proportional to its content in the feed solution. Accordingly, to provide a higher driving force, an NH_3-concentrated feed solution is favoured.

Raoult's Law

Raoult's Law is used to determine the vapour pressure of a component (i) in an ideal solution (a solution in which solvent-solvent and solvent-solute interaction are identical) as a function of vapor pressure of the saturated vapor pressure of i and its mole fraction in the solution (Lide et al., 2009):

$$P_i = \chi_i \cdot P_i^* \qquad Eq.17$$

P_i – partial pressure of component i, [Pa];

χ_i – mole fraction of i in the solution [-];

P_i^* - saturated vapor pressure of i, [Pa].

In ideal dilute solutions, solvent strictly obeys Raoul's law meaning the purer the solution the better it obeys. Though solutions in this study is non-ideal, Raoult's law is considered valid as a rough approximation for partial pressure of H_2O. It generally shows that keeping a low water mole fraction in a solution is beneficial for selective transport of NH_3 in terms of driving force.

2.4.2 Permeate Side - Dalton's Law & Ideal Gas Law

Dalton's Law states that the total pressure (P_{total}) of a gas mixture is the sum of the partial pressure (P_i) of each component. For an ideal gas (no interaction among gas molecules) that follows the ideal gas law $(PV = nRT)$, Dalton's Law can be expressed as $Eq.18$ (Nivaldo, 2014):

$$P_{total} = \Sigma P_i = n_{total}\frac{RT}{V} \qquad Eq.18$$

where

P_{total} – total pressure of a gas mixture, [Pa];

P_i – partial pressure of gas i, [Pa];

n_{total} – sum of mole of each component in the gas mixture, [mole];

R – universal gas constant, 8.314 [J·mol^{-1}·K^{-1}];

T – temperature of the gas mixture, [K];

V – volume of the gas mixture, [m^3].

By means of a simple deduction, the relation between the partial pressure of a single component and the total pressure can be derived as shown in Eq. 19:

$$P_i = \chi_i \cdot P_{total} \qquad Eq.\ 19$$

in which

χ_i – mole fraction of gas i in the gas mixture, [-].

According to this, the partial pressures of NH_3 and H_2O at the permeate side can be obtained by knowing their mole fractions.

2.4.3 Fugacity

For a gas mixture, in a non-ideal situation, due to the interaction among gas molecules, its pressure presented is, in fact, lower than that of an ideal situation. A term, fugacity (f_i), is employed to describe the effective pressure for a non-ideal gas as pressure is for an ideal gas (Lide et al., 2009). The correction for ideal gas to non-ideal gas is approached using fugacity coefficient ($\varphi_{i,(T)}$) which is a gas-specific and temperature-dependent coefficient and is equal to unity for ideal gas:

$$f_i = \varphi_{i,(T)} \cdot P_i \qquad Eq.\,20$$

Considering this, to acquire the actual partial pressures of NH_3 and H_2O at membrane feed and permeate sides, fugacity should be applied for calculation rather than pressure. According to Holley et al. (1958), in the temperature range of this study, the fugacity coefficients for NH_3 and H_2O are both close to unity. Therefore, the vapour pressure of each species were directly used as the actual partial pressure for calculation.

2.5 Chemical Equilibrium

2.5.1 Equilibrium Constant

Consider a general reversible chemical reaction:

$$aA + bB \leftrightarrow cC + dD \qquad Eq.21$$

The overall reaction can proceed in both forward and reverse directions as a response to changes such as concentrations, temperature, pressure and etc. For a given ambient condition, a dynamic equilibrium state will eventually be established, where the rate of the forward reaction equals the rate of reserve reaction. At this equilibrium state, the distribution of reactants and products is given by a equilibrium constant K, which is defined in Eq. 22:

$$K = \frac{[C]^c[D]^d}{[A]^a[B]^b} \qquad Eq.22$$

where

$[C], [D]$, $[A]$ and $[B]$ – activities of products and reactants at equilibrium, [mol·L^{-1}] (see section 2.5.3);

a, b, c and d – stoichiometric coefficients of corresponding components;

The value of the equilibrium constant is related to the thermodynamic properties of both reaction system and involved chemicals. At standard condition (25 °C, 1.0 bar), the equilibrium constant K° can be calculated via the standard Gibbs free energy using Eq. 23:

$$K^\circ = e^{\frac{-\Delta_r G^\circ}{R \cdot T^\circ}} \qquad Eq.23$$

in which,

$\Delta_r G^\circ$ – standard Gibbs Free Energy, [kJ·mol^{-1}];

R – universal gas constant, 8.314 [J·mol^{-1}·K^{-1}];

T° – temperature at standard condition, 298.15 [K];

For non-standard conditions, the equilibrium constant (K_T) at temperature T can be derived from the equilibrium constant at standard condition using Van't Hoff equation:

$$K_T = K^\circ \cdot e^{\frac{-\Delta_r H^\circ}{R}\cdot(\frac{1}{T}-\frac{1}{T^\circ})} \qquad Eq.24$$

$\Delta_r H^\circ$ - Standard enthalpy of a reaction, [kJ·mol^{-1}];

2.5.2 Water Equilibrium

The dynamic equilibrium of water molecules is a universal equilibrium existing in almost every aqueous solution:

$$H_2O_{(l)} \leftrightarrow H^+{}_{(aq)} + OH^-{}_{(aq)} \qquad Eq.25$$

$K^\circ_{H_2O_{(l)}} = 1.00 \cdot 10^{-14}$ (Hendricks, 2006; Stumm et al., 2012)

When ammonia is presenting in aqueous solution, besides being dissolved as gas (Eq. 27), it immediately interacts with water molecules forming ammonium hydroxide, a weak base solution (Eq. 26):

$$NH_{3(aq)} + H_2O_{(l)} \leftrightarrow NH_4^+{}_{(aq)} + OH^-_{(aq)} \qquad Eq.26$$

$K^\circ_{NH_{3(aq)}} = 1.79 \cdot 10^{-5}$ (Anthonisen et al., 1976; Helgeson, 1967)

$$NH_{3(aq)} \leftrightarrow NH_{3(g)} \qquad Eq.27$$

If ammonia is present as ammonium bicarbonate, as aforementioned the primary ammonium salt in reject water, equilibria regarding bicarbonate are introduced:

$$HCO^-_{3(aq)} + H^+{}_{(aq)} \leftrightarrow CO_3^{2-}{}_{(aq)} + 2H^+{}_{(aq)} \qquad Eq.28$$

$K^\circ_{HCO^-_{3(aq)}} = 4.68 \cdot 10^{-11}$ *(Moel et al., 2006)*

$$CO_{2(aq)} + H_2O_{(l)} \leftrightarrow HCO^-_{3(aq)} + H^+{}_{(aq)} \qquad Eq.29$$

$K^\circ_{CO_{2(aq)}} = 4.62 \cdot 10^{-7}$ *(Stumm et al., 2012)*

$$CO_{2(aq)} \leftrightarrow CO_{2(g)} \qquad Eq.30$$

These reversible chemical equilibria result in a fact that the CO_2 is also presented in the gaseous state. According to the mass transfer mechanism of pervaporation, CO_2 can also be transported because of the existence of driving force. This will reduce the mass fraction of NH_3 in the permeate side which is undesirable. However, because these reversible reactions are sensible to ambient conditions: any fluctuation in temperature, concentrations, pH and pressure will shift these dynamic equilibria, action can be taken to reduce the partial pressure of CO_2 preventing

the potential permeating of CO_2. Adjusting the pH is usually the most straightforward method and, based on Eq. 25 - Eq. 30, alkaline environment is favoured.

Figure 7 displays the distribution of total inorganic carbon (TIC) and TAN (total ammonia nitrogen) under various pH, which were the results of PHREEQC simulations (based on 0.5 M NH_4HCO_3, pH adjusted by either HCl or $NaOH$). It can the seen that when pH is above 10, most inorganic carbon is present as carbonate ions (CO_3^{2-}) and free NH_3 dominates TAN. In other words, pH 10 is the minimum level to avoid gaseous TIC (i.e. CO_2). However, when further increasing the pH above 10, the increase of the amount of NH_3 is limited. Hence, in this study, pH was fixed at 10 for all ammonia bicarbonate (AmmBiC case) experiments.

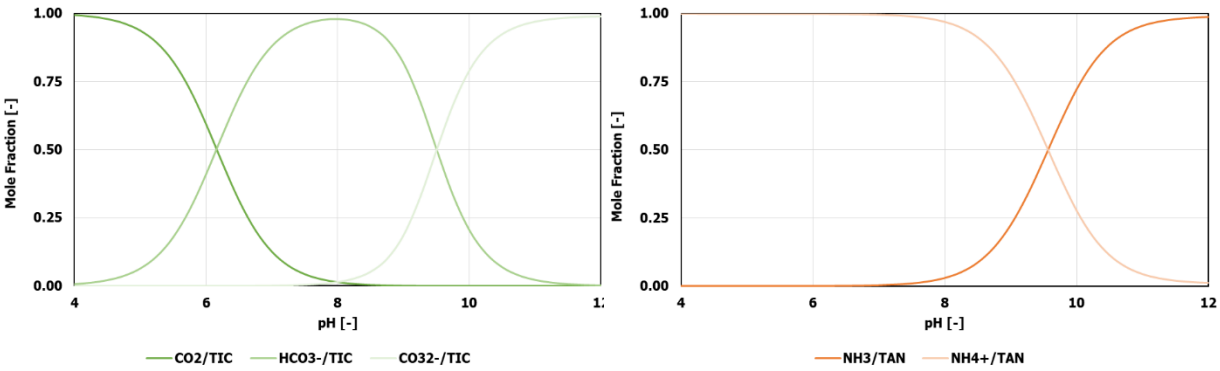

Figure 7 Species distribution of 0.5 M ammonium bicarbonate solution under various pH at 25°C. a) Total inorganic carbon (TIC) distribution over pH; b) TAN distribution over pH.

2.5.3 Activity

Electrostatic Shielding Effect and Salting Out Effect

In a non-ideal solution, a dissolved ion is usually surrounded by water molecules forming a so-called hydrate complex. Because of this water shell, this ion is unable to participate into chemical reactions or be measured effectively resulting in an actual concentration of the ion less than its theoretical element concentration. This phenomenon is well-known as the electrostatic shielding effect (Appelo et al., 2004).

Salting-out effect describes the phenomenon that, as the salinity of a solution increases, a growing amount of water molecules acts as shield surrounding dissolved ions so that less water molecules are available for dissolving salt. In particular, in this study, salting-out means less available water molecules to dissolve ammonia gas.

Both effects affect the number of free molecules or ions that can effectively join chemical reactions, hence correction is necessary.

Activity

Activity, (a_i), is a correction for the loss of reactivity of ions due to the electrostatic shielding and salting-out effects in terms of activity coefficient (γ_i):

$$a_i = \gamma_i \cdot c_i \qquad Eq.31$$

The activity coefficient depends on the ionic strength (I) of the solution which can be calculated by Eq. 32:

$$I = \frac{1}{2}\sum c_i z_i^2 \qquad Eq.32$$

where,

z_i – electric charge of ion i, [-];

c_i – concentration of ion i, [mol·L^{-1}].

The relation between activity coefficient (γ_i) and ionic strength (I) can be quantified by several equations. For dilute solution (I < 0.5 mol·kg^{-1}) Davies equation is usually applied (Appelo & Postma, 2004):

$$log\gamma_i = -A_T z_i^2 \frac{\sqrt{I}}{1+\sqrt{I}} - 0.3I \qquad Eq.33$$

While Truesdell and Jones equations can be applied when I < 1 mol·kg^{-1} (Appelo & Postma, 2004):

$$log\gamma_i = \frac{-A_T \cdot z_i^2 \cdot \sqrt{I}}{1 + B_T \cdot a_i \cdot \sqrt{I}} + b_i \cdot I \qquad Eq.34$$

Where,

z_i - electric charge of ion i, [-];

A_T, B_T - Temperature dependent parameters, [-];

a_i, b_i- ion-specific fit parameters (dependent on the ion radius).

It should be noted that increasing salinity has two opposite effects on P_{f,NH_3}. One the one hand, less ammonia gas can be dissolved due to the salting-out effect, which is positive for the driving force. However, on the other hand, when the salinity of feed solution increasing (i.e. I increasing), the activity of NH_3 increasing. According to the equilibrium of NH_3 and NH_4^+ in liquid solution ($Eq.26$), the ionization of NH_3 is enhanced, which is negative for the driving force. PHREEQC simulation showed for NH_3, the salting-out effect is more significant than the ionization. Nevertheless, the impact of salt on NH_3 transfer in the pervaporation process is unclear.

3 Methods and Materials

3.1 Operational Conditions

To study the selective transport of NH_3 by silica-based ceramic pervaporation membrane, four case studies were executed in order of solution complexity.

Demi-water case was conducted to determine critical Reynolds numbers of the membrane configuration applied in this study. Salt case aimed at estimating the salt impact on H_2O transfer. The other two cases focussed on NH_3 transfer. AmmOH case was designed to acquire the optimum temperature and flow regime for selective NH_3 transport by studying the impact of temperature and flow regime. Meanwhile, in this case, the impact of TAN concentrations was also evaluated as a reference for AmmBiC case of which NH_3 transfer was disturbed by additional salt. Finalized experimental conditions are summarised in Table 1 with detailed elaboration in the following sections.

Table 1 Finalised experimental condition matrix

Case Name	Salt Type	Temperature	Salt Concentration	Reynolds Number					pH Adjustment
[-]	[-]	[°C]	[g·L^{-1}] or [g TAN·L^{-1}]	[-]					
				1,000	2,400	3,000	4,000	5,000	
Demi-water	None	35	0.0	√	√	√	√	√	without
Salt	$NaCl$	35	50.0		√				
			100.0		√				
AmmOH	NH_4OH	45	1.5		√		√		
		35	1.5	√	√		√		
			12.0		√		√		
			20.0		√				
AmmBiC	NH_4HCO_3 + $NaOH$	35	1.5		√				till 10
			12.0		√				
			20.0		√				

3.1.1 Reynolds Number

As explained in section 2.1, that the flow regime is of great importance in pervaporation mass transfer process. Since the critical Reynolds numbers used to define the flow regime are geometry-dependent, the main task of the demi-water case, in this research, was to identify these numbers for the membrane configuration employed. For a tubular flow type, Re=2,400 and Re=4,000 are commonly regarded as critical numbers to distinguish the flow regime: within the two limits, it is transition flow; below the range is laminar flow otherwise called turbulent flow (Munson et al., 2014; Oliveira et al., 2001). Considering this, in this study, Reynolds number equals to 2,400 and 4,000 plus 1,000, 3,000 and 5,000 were selected for testing. Furthermore, it was assumed that laminar or turbulent flow was achieved when water flux (J_{H_2O}) at two consecutive points were almost identical. For example, if J_{H_2O} at Re=1,000 equals J_{H_2O} at Re=2,400, and both are smaller than J_{H_2O} at Re=3,000, Re=2,400 is considered as one critical Reynolds number.

3.1.2 pH

Experiments fed with ammonium hydroxide (NH_4OH) solution were conducted at its natural pH around 11.5. Whereas the pH of the NH_4HCO_3 solutions used in AmmBiC case were adjusted up to 10.0±0.2, as elaborated in section 2.5, to increase the mole fraction of free NH_3 in the liquid phase and to restrain the gasification of CO_2.

3.1.3 Solutions

To explore the impact of NH_3 concentration on the selective transport of NH_3 by silica-based ceramic pervaporation membrane, three TAN concentrations were employed for testing. They were 1.5, 12.0 and 20.0 g TAN·L^{-1}, respectively. Reasons being that 1.5 g TAN·L^{-1} is the TAN concentration in the reject water of a typical anaerobic digester; 12.0 g TAN·L^{-1} is the TAN concentration in the effluent of pre-treatment process considered in the "N2kWh-From pollutant to power" project; 20.0 g TAN·L^{-1} was for extrapolating the result to a higher NH_3-concentrated streams like industrial wastewater or concentrated urine.

It should be noted that Na^+ would be inevitably introduced when $NaOH$ is used to adjust the pH of NH_4HCO_3 solution. The amount of this additional ion depends on the initial TAN concentration. In principle, studying the impact of TAN concentration on NH_3 transfer by simply increasing the amount of NH_4HCO_3 is scientifically inappropriate because salt would play a role in the mass transfer. Hence, the main task of the salt case was to estimate the impact of the presence of salt on H_2O transfer as the base case for analyzing its impact on NH_3 transfer.

A preliminary PHREEQC simulation showed increasing the pH of 12.0 and 20.0 g TAN·L^{-1} NH_4HCO_3 solutions to 10 would consume 0.85 and 1.71 mol·L^{-1} of $NaOH$, respectively. Corresponding to the required level of $NaOH$, 50 g·L^{-1} and 100 g·L^{-1} of $NaCl$ were tested accordingly to provide a similar ionic strength.

3.1.4 Temperature

A PHREEQC simulation on solutions containing various TAN concentrations indicated that in a lower temperature range (1-100 °C), 35 °C was the optimum temperature for separating NH_3 from liquid solution due to a relatively high ratio of partial pressure of NH_3 to the partial pressure of H_2O (see Figure 8). Hence, 35 °C was considered in the experiments.

Besides, the mass transfer mechanism and the heat transfer mechanism show that temperature will affect not only the driving force but also the solubility and diffusivity of permeate inside the membrane structure. However, in the literature results on the latter impact are ambiguous. To this end, 45 °C was selected.

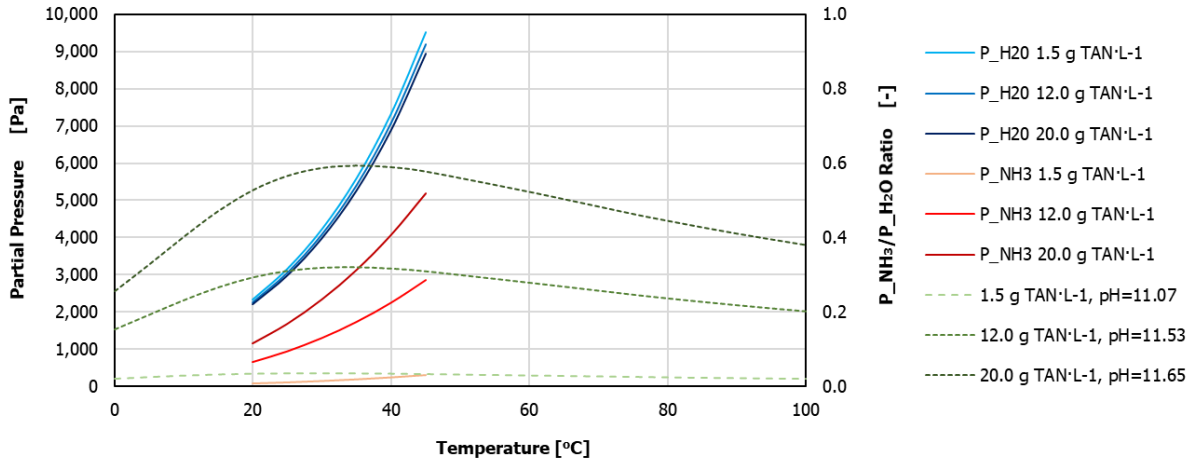

Figure 8 Results of PHREEQC simulations on ammonia and water partial pressure in various solutions

3.2 Synthetic Solution

Each experiment started with the same initial volume of feed solution. That was 500 mL.

The solution used in the demi-water case was pure demi-water (EC<2 µS·cm^{-1}). For the other cases, feed solutions were prepared by either dissolving sodium chloride ($NaCl$, ⩾98%, VWR Prolabo), or diluting ammonia hydroxide (NH_4OH, ca. 25%, Acros-Organics), or dissolving ammonia bicarbonate (NH_4HCO_3, ⩾99.5%, Sigma – Aldrich) with pre-heated demi-water. In addition, for AmmBiC case, pH was adjusted using sodium hydroxide solution ($NaOH$, ca. 32%, BOOM BV, the Netherlands).

Acidic trap containing 200 mL of 0.5 M sulfuric acid was diluted from 2.5 M sulfuric acid (H_2SO_4, Merck KGaA) using demi-water.

3.3 Pervaporation Membrane

Two types of commercial silica-based ceramic pervaporation membranes, manufactured by Pervatech BV, the Netherlands, were investigated in this study. Hybrid Silica AR membrane, with a length of 25 cm and an effective area of 0.005 m^2, has a tubular configuration with an inner diameter of 7 mm. The hybrid silica layer (i.e. the active layer) exhibiting hydrophilic surface property is inner-coated on $\alpha - Al_2O_3$, the substrate material. So, the feed flows inside the membrane tube while permeate is collected at the outside. As visualized in Figure 9, the acute contact angle confirms its hydrophilicity. The pore size of this active layer varies between 0.3 and 0.5 nm (Yang et al., 2016).

PDMS (Poly Di Methyl Siloxane) pervaporation membrane has the same dimensions as the Hybrid Si AR membrane except a different active layer which is coated with hydrophobic PDMS.

At the end of each experiment, to clean the membrane, fluxing was conducted using demi-water. After that, the membrane was preserved in a dry ambient environment to avoid the growth of fungi.

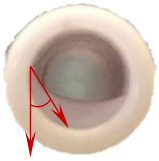

Figure 9 Impression of water drop distributed on Hybrid Si PV membrane.

3.4 Pervaporation Apparatus

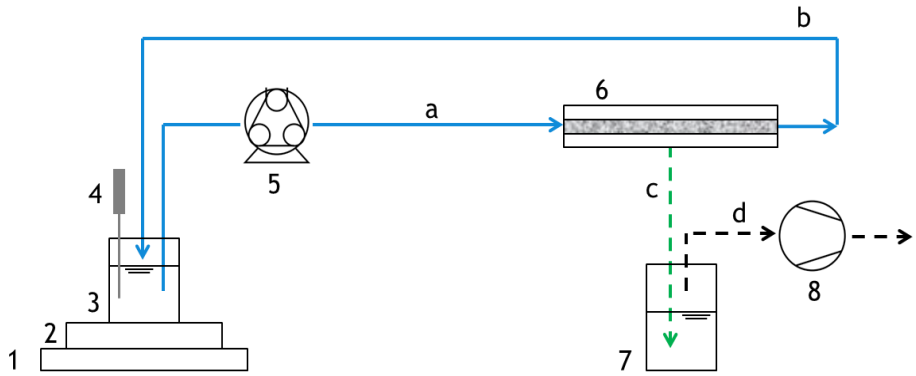

Figure 10 Schematic diagram of experimental apparatus used in this study.

	Equipment		Streams
1.	Digital Balance	a.	Liquid Feed Stream
2.	Magnetic Stirring Heating plate	b.	Liquid Dilute Stream
3.	Feed Solution Bottle	c.	Gas Permeate Stream
4.	Sensor (EC, pH and Temperature)	d.	Gas Vacuum Stream
5.	Peristaltic Pump		
6.	Membrane Housing		
7.	Cold Acid Trap		
8.	Vacuum Pump		

The experiments in this study were carried out with a lab-scale cross-flow membrane unit, as schematically shown in Figure 10. The feed solution was supplied by a peristaltic pump (520S, Watson Marlow) to a membrane held by a stainless-steel housing where ammonia stripping occurred. After stripping, the liquid retentate was returned to the feed bottle. A magnetic stirring heating plate (RH Digital KT/C, IKA) was employed to control the temperature and to distribute feed concentration evenly. Beneath the heating plate was a bench-scale digital balance (PCB, KERN) of which readings can be logged to a laptop automatically during every experiment. Properties (temperature, EC and pH) of every tested solution were measured via a multi-meter (Multi 3630 IDS, WTW) with calibrated sensors. As for the permeate side of the membrane, the pressure was constantly maintained at 1,500 Pa (absolute pressure) by a vacuum pump (N 816.3KN. 18, KNF, Germany) located after a wash bottle. 200 mL of sulfuric acid solution (0.5 M) was stored in this wash bottle to collect permeated H_2O and NH_3 and to avoid NH_3 intruding upon the vacuum pump. Additionally, the temperature of the acidic solution was constant at 0 °C to accelerate the condensation of H_2O and to minimize the evaporation of this acidic solution that might perplex the analysis in terms of partial pressure at the permeate side.

3.5 Experimental Procedure

Before starting, at least one hour was considered for conditioning when a dry membrane was applied (Hirabayashi, 2002). Meanwhile, the solution was pre-heated to a desired temperature. During the experiment period (1 to 1.5 hours in total) samples were pipetted directly from the feed water bottle in a time interval of 15-20 minutes. The total weight of the feed water bottle and the heating plate was recorded at a frequency of 30 seconds. The multi-meter adopted the same frequency to measure electrical conductivity, temperature and pH occasionally.

TAN concentration (presented as NH_3, i.e. c_{NH_3}) of each sample was measured via Nanocolor® 2000 kits and spectrophotometer NANOCOLOR® VIS (Macherey-Nagel, Germany). Dilution was executed when the concentration of the feed solution was too high to be measured by this kit. Moreover, samples were stored no more than 30 minutes before this spectral analysis.

For each case study, each combination of operating conditions was performed in triplicate.

3.6 Analytical Methods

3.6.1 Flux

For each sampling period, t_n to t_{n+1}, the flux was calculated by Eq. 35:

$$J = \frac{\Delta m_i}{\Delta t \cdot A} \qquad Eq.\ 35$$

in which,

Δm_i – mass difference between t_n and t_{n+1}, i represents H_2O or NH_3 or total mass, [kg];

Δt – time slot, [h];

A – effective membrane area, 0.005 [m^2];

$$m_{total,t_n} = m_{H_2O,t_n} + m_{NH_3,t_n} + m_{salt} \qquad Eq.\ 36$$

$$m_{NH_3,t_n} = c_{NH_3,t_n} \cdot V_{t_n} \qquad Eq.\ 37$$

$$V_{t_n} = \frac{m_{total,t_n}}{\rho} \qquad Eq.\ 38$$

where,

m_{total,t_n} – total mass at t_n, [kg];

c_{NH_3,t_n} – NH_3 concentration at t_n, [kg·L^{-1}];

V_{t_n} – total volume of feed solution at t_n, [L];

ρ – density of feed solution, [kg·L^{-3}].

The initial m, m_{salt}, V and ρ were known once the solution was prepared. m_{salt} and ρ were assumed to remain the same during the run of an experiment; m_{total} and corresponding time (t_1, t_2…) was consciously logged via the digital scale; c_{NH_3} of each sample was provided by kits (see section 3.5).

3.6.2 Driving Force

In this study, the partial pressure of H_2O and NH_3 at the membrane feed side were determined by PHREEQC Interactive (3.4.0). This software not only considers aforementioned chemical equilibria but also provides the partial pressure in terms of fugacity as a function of corresponding saturation index integrating all aforementioned laws when temperature and concentrations are known. As discussed in section 2.4.3, for both H_2O and NH_3, since fugacity coefficient is close to unity, fugacity equals partial pressure.

As for the partial pressure of H_2O and NH_3 at the permeate side, they were determined based on Dalton's law. Since the total pressure at the permeate side was constant at 1,500 Pa, the partial pressure of H_2O and NH_3, therefore, depended on its mole fraction (See section 2.4.2), which can be obtained:

$$\chi_{NH_3} = \frac{J_{NH_{3,t_n}}}{J_{NH_{3,t_n}} + J_{H_2O,t_n}} \qquad Eq.\ 39$$

$$\chi_{H_2O} = 1 - \chi_{NH_3} \qquad Eq.\ 40$$

in which,

χ – mole fraction, [-];

J – molar flux, [mol·m^{-2}·h^{-1}];

In addition, it was assumed that the performance of the silica-bases ceramic pervaporation membrane tested during two consecutive sampling points was stable. In other words, for example, at either the feed side or permeate side, though partial pressure of NH_3 was calculated for each sampling time respectively, the value used for analysis was the average partial pressure based on the two successive sampling points. The same for H_2O partial pressure.

3.6.3 Mass Transfer Coefficient

Once the flux and the driving force were obtained, the overall mass transfer coefficient can be calculated by rewriting Eq. 1:

$$k_{ov} = \frac{J}{(P_f - P_p)} \qquad Eq.\ 41$$

3.6.4 Perm-selectivity

In the pervaporation literature, there are several terms employed to assess the capability of a pervaporation membrane for permeating certain species. Concentration factor, enrichment factor, selectivity, perm-selectivity and etc. are commonly used, but definitions of those terms are rather ambiguous (Böddeker, 1990; Cheng et al., 2017; Jyoti et al., 2015; Lipnizki et al., 1999; Vane, 2005).

In this study, the ability of silica-based ceramic pervaporation membrane for selective transport of NH_3 was estimated by perm-selectivity, α, which is defined as the ratio of permeabilities of permeates (i.e., NH_3 and H_2O). It was employed because it reveals the intrinsic difference in selective transport of H_2O and NH_3 by the membrane material excluding the influence from driving force. Since the thicknesses of the two types of membrane used in this study were identical, perm-selectivity could be expressed as:

$$\alpha = \frac{k_{ov,NH_3}}{k_{ov,H_2O}} \qquad Eq.\ 42$$

α equals unity means the membrane equally transport H_2O and NH_3. α greater than one means NH_3 is more selectively transported than H_2O otherwise H_2O is more selectively transported.

3.6.5 Concentration Factor

The concentration factor (β), being the ratio of NH_3 mole fraction in the permeate and the feed solution was also calculated to estimate the quality of permeate:

$$\beta = \frac{n_{NH_3 permeate}}{n_{NH_3 feed}} \qquad Eq.\ 43$$

Considering 1.5 wt% of NH_3 in the feed solution while 5 wt% is required for directly use in SOFC (i.e. 5 w% of NH_3 in the permeate), β at least 33 is desired.

3.6.6 Energy Consumption

In principle, energy in pervaporation process is only required in order to achieve the phase change of permeate species (El-Bourawi et al., 2006; Lawson et al., 1997). In this study, it was the latent heat consumed by permeating H_2O and NH_3. The energy consumption (i.e. heat flux) for of each permeate species can be calculated by:

$$Q_i = J_i \cdot \Delta H_i \qquad Eq.\ 44$$

where

Q_i – heat flux, [MJ·m^{-2}·h^{-1}]

J_i – flux of i, [kg·m^{-2}·h^{-1}];

ΔH_i – enthalpy change of i , [MJ·kg^{-1}].

At standard condition the enthalpy change of H_2O ($\Delta H_{vap,H_2O}$) is +2.44 MJ·kg^{-1} ;and the enthalpy change of NH_3 ($\Delta H_{vap,NH_3}$) is +1.79 MJ·kg^{-1} at 35.7 °C and 1.0 bar (Lide et al., 2009). According to Nivaldo (2014), the change of

$\Delta H_{vap,H_2O}$ over temperature is minor (about 0.16 MJ·kg^{-1}, from 25 °C to 100 °C), an assumption had been made that in the temperature range from 25 °C to 35 °C , the change of $\Delta H_{vap,H_2O}$ was negligible and the same for $\Delta H_{vap,NH_3}$ meaning constant values were emplloyed for analysis.

To answer the second research question regarding energy consumption, the theraml energy consumed by permeating per kilogram of N through pervaporation in this study was calculated by:

$$\Delta H'_{NH_{3-N}} = \frac{J_{NH_3} \cdot \Delta H_{vap,NH_3} + J_{H_2O} \cdot \Delta H_{vap,H_2O}}{J_{NH_3}} \cdot \frac{14}{17} \qquad Eq.\ 455$$

in which,

$\Delta H'_{NH_{3-N}}$ – consumed thermal energy by pervaporation of NH_3, [MJ·kg^{-1} -N];

J – flux, [kg·m^{-2}·h^{-1}].

$14, 17$ – molecular wight of N and NH_3, respectively, [g·mol^{-1}]

3.7 General Assumptions

To simplify the research, three general assumptions were made as follows:

1. Heat loss of the experimental setup was negligible meaning that the temperature of feed solution inside the membrane module was equal to the temperature of the solution in the feed bottle;
2. For the experiments aiming at finding out the critical Reynolds numbers (i.e. demi-water case), the influence of concentration polarization effect was ignored meaning that the change in water flux, could be attributed to the influence of flow regime on temperature polarization;
3. Change in the density of the feed solution was neglected during one run of experiment meaning that the density used for calculation was equal to the initial solution.

3.8 Hypothesis

According to the foregoing theoretical background, the hypotheses with respect to each specific research questions (section 1.6) are proposed in this section. Notably, hypotheses related to flux were deduced based on the driving force provided by PHREEQC simulation results (see Table 3) with ignorance of partial pressure at the membrane permeate side (P_p).

Table 2 Hypotheses of each case study

Research question and Variables	Parameter	Hypothesis	permeated sepcies	k_{ov}						P_f
				k_f				k_m		
				Concentraiton Polarization		Temperature Polarization	Resistance	solubility	Diffusivity	
				depletion	accumulation					
1.a Flow regime	J	↑	NH_3	↓	-	↓				↑
		↑	H_2O	-	-	↓				↑
	k_{ov}	↑	NH_3						↑	
		↑	H_2O						↑	
	α	↕								
1.b Temperature	J	↑	NH_3	↑	-	↑				↑
		↑↑	H_2O	-	-	↑				↑↑
	k_{ov}	↑	NH_3						↑	
		↑	H_2O						↑	
	α	↕								
1.c TAN concentration	J	↑	NH_3	↕	-					↑
		↓	H_2O	-	-		↑			-
	k_{ov}	↕	NH_3							
		↓	H_2O				↑			
	α	↕								
1.d Salt	J	↑	NH_3	-	↑		↑			↑
		↓	H_2O	-	↑		↑			↓
	k_{ov}	↓	NH_3		↑		↑			
		↓	H_2O		↑		↑			
	α	↕								

↑	increase	*green*	positive for mass transfer
↓	decrease	*red*	negative for mass transfer
↕	decrease or increase	*blue*	unpredictable
-	*being not significantly affected*		

Table 3 Ammonia and water partial pressure corresponding to every tested feed solution

Salt Type	Temperature [°C]	TAN Concentration [g TAN·L^{-1}]	NH_3 [Pa]	H_2O [Pa]	$P_{f,NH_3}/P_{f,H_2O}$ [-]
NH_4OH (natural pH)	35	1.5	211	5,621	4 %
		12.0	1,705	5,564	31%
		20.0	2,846	5,522	52%
	45	1.5	323	9,552	3 %
		12.0	2,612	9,456	28%
		20.0	4,361	9,385	46%
NH_4HCO_3 (pH adjusted to 10 by $NaOH$)	35	1.5	196	5,599	3 %
		12.0	1,736	5,407	32%
		20.0	3,132	5,268	59%
	45	1.5	316	9,515	3 %
		12.0	2,848	9,186	31%
		20.0	5,175	8,946	58%
$NaCl$	35	0.0		5,495	
		50.0		5,370	
		100.0		5,248	

Research question 1.a – Flow Regime

It was hypothesized that, as the flow regime shifted from laminar flow to fully turbulent, J_{H_2O} and J_{NH_3} would increase due to a positive impact of flow regime on the driving force. More explicitly, at the feed side, both P_{f,H_2O} and P_{f,NH_3} were expected to increase because polarization effects were diminished by a more turbulent flow.

Based on current knowledge, the diffusivity is positively related to temperature (Jyoti et al., 2015). Supposing the solubility remained the same for both H_2O and NH_3, as the difference between T_i and T_f reducing (i.e. more turbulent flow), k_{ov,NH_3} and k_{ov,H_2O} would increase accordingly. However, α was unpredictable because it was unknown that how and to which extend would the solubility and k_{ov} be affected for both components.

Research question 1.b – Temperature

It was hypothesized that the overall impact of temperature on J_{H_2O} and J_{NH_3} were positive. Moreover, the increase of J_{H_2O} would be more than that of J_{NH_3} because P_{f,H_2O} would increase more than P_{f,NH_3} as the temperature increasing (see Table 3 and Figure 8). However, it should also be noted that as J_{total} increasing, there would be a growing negative impact from temperature polarization for both J_{H_2O} and J_{NH_3}. Besides, the depletion type of concentration polarization effect was possible to be intensified resulting from the increase of J_{NH_3}.

Similar to the impact of flow regime, the impact of temperature on α was also unpredictable due to the uncertainly of the extent to which k_{ov,NH_3} and k_{ov,H_2O} would be affected.

Research question 1.c – TAN Concentration

Based on the results of PHREEQC simulation on p_f (Table 3), as the TAN content in the feed solution increasing, P_{f,NH_3} increased significantly while P_{f,H_2O} presented a slightly decrease. Accordingly, J_{NH_3} was expected to increase while J_{H_2O} was to decrease. Another reason for the decrease of J_{H_2O} was a possible increase of resistance for H_2O transfer since more NH_3 molecules were presenting in the environment.

As for α, since the impact of TAN concentration on k_{ov} was uncertain for both species because of the unknown changes of k_m and k_f, how would α be affected was unpredictable.

Research question 1.d – Additional Salt

As indicated in Table 3, in general, P_{f,NH_3} increase because of the presence of additional salt whereas P_{f,H_2O} decreases. So that, expect AmmBiC 1.5 g TAN·L^{-1} case, J_{NH_3} was expected to increase while J_{H_2O} decrease.

However, the presence of salt would possibly increase the resistance of mass transfer (i.e. more severe accumulation type of concentration polarization). Consequently, k_{ov,NH_3} and k_{ov,H_2O} were expected to decrease to an uncertain extent resulting an unpredictable α.

4 Results and Discussion

4.1 Hydrophobic PDMS PV Membrane

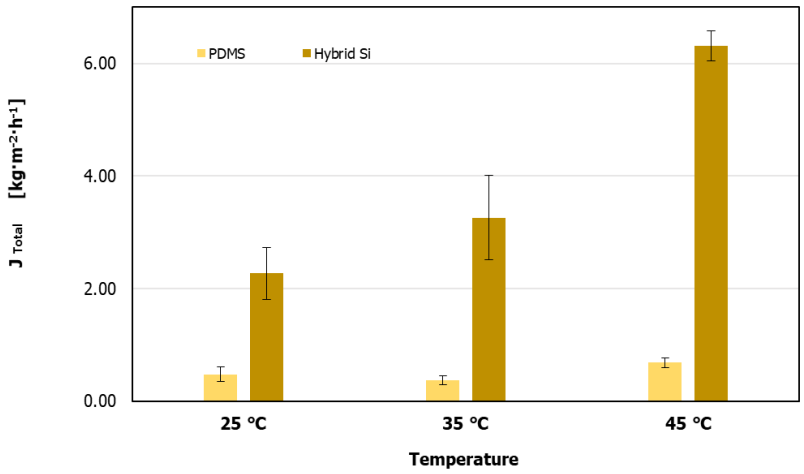

Figure 11 Total flux of PDMS hydrophobic PV memrbane fed with demi-water at Re 2,400. Error bars represent standard deviation of trplicate experiments.

Figure 11 shows the total flux produced by Hybrid Si AR (hydrophilic) and PDMS (hydrophobic) membranes fed with demi-water. At 25 °C, J_{Total} of PDMS membrane was 80% lower than that of Hybrid Si membrane. Noteworthy, this number was 90% when temperature increased from 25 to 35 and further to 45 °C. This significant difference in J_{Total} indicated that hydrophobic PDMS membrane can block H_2O effectively preventing the increase of J_{Total} due to increased driving force.

Nonetheless, when PDMS membrane was exposed to experimental solution (1.5 g TAN·L^{-1}, AmmOH, without pH adjustment, 35 °C, Re=2,400), results (see Table 4) showed that the PDMS membrane not only water-phobic but also ammonia-phobic to a certain degree.

Table 4 Performance of the PDMS PV memrbaen on ammonia stripping over time (1.5 g TAN·L^{-1}, AmmOH)

Time	α	J			k_{ov}	
		Total	NH_3	H_2O	NH_3	H_2O
[h]	[-]	[kg·m^{-2}·h^{-1}]			[s·m^{-1}]	
0.25	0.11	4.73	0.02	4.71	3.44E-08	3.17E-07
0.50	0.09	2.11	0.01	2.10	1.31E-08	1.41E-07
0.75	0.13	1.35	0.01	1.35	1.17E-08	9.06E-08
1.00	3.73	0.70	0.04	0.66	1.62E-07	4.34E-08
1.50	0.41	0.60	0.01	0.59	1.62E-08	3.99E-08

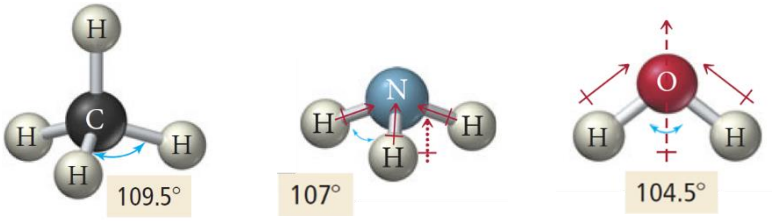

a) b) c)

Figure 12 Molecular Geometries. a) CH_4; b) NH_3; c) H_2O. Adapted from (Nivaldo, 2014)

The "like dissolves like" theory can explain the phenomenon that PDMS not only prevented H_2O but also prevent NH_3. This rule of thumb theory describes the fact that polar and nonpolar molecules do not mix (Nivaldo, 2014). In other words, polar molecules can only mix with polar molecules and vice versa. As depicted in Figure 12, both NH_3 and H_2O are polar molecules because of their unevenly distributed polar bonds compared with nonpolar molecules such as methane (CH_4). Accordingly, the reason why PDMS membrane could not allow H_2O to pass was PDMS is nonpolar whereas H_2O is polar. Similarly, NH_3 as a polar molecule would be prevented by PDMS membrane either. In chemistry, electrical dipolar moment, in [D], is commonly used to quantify the polarity of molecules. The net electrical dipolar moment for NH_3 and H_2O are 1.47 D and 1.85 D, respectively (Miessler et al., 2014). Nevertheless, the results of k_{ov,H_2O} and k_{ov,NH_3} showed this difference could hardly result in a selective transport of either component, at least by PDMS PV membrane.

In addition, the PDMS membrane exhibited poor stability under alkaline environment (see Table 4), that is: during the 1.50-hour run time, J_{total} and α fluctuated so much making analysis impossible. Besides, a fluffy deterioration of the active PDMS layer was detected a week after the first experiment with ammonia solution (Figure 13), which rejected the attempt for a duplicate experiment on PDMS PV membrane. The following experiments were conducted using Hybrid Silica pervaporation membrane.

Figure 13 Deteriorated PDMS pervaporation membrane

4.2 Demi-Water Case Study

4.2.1 Critical Reynolds Number

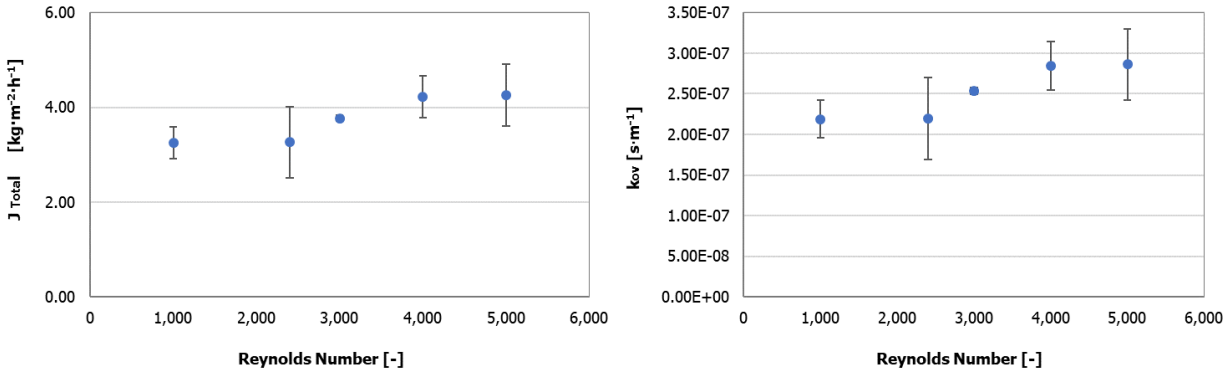

Figure 14 Results of demi-water case: a) water flux over Reynolds number; b) overall water transfer coefficient over Reynolds number. Error bars represent the standard deviation of triplicate experiments.

Figure 14 shows the changes of water flux (J_{H_2O}) and mass transfer coefficient (k_{ov,H_2O}) under various Reynolds numbers, in which an S-shaped curve of both J_{H_2O} and k_{ov,H_2O} can be observed: J_{H_2O} remained stable at 3.26 kg·m^{-2}·h^{-1} in the Reynolds number range of 1,000 to 2,000 followed by an ascending trend until reaching a plateau (4.23 kg·m^{-2}·h^{-1}) at Reynolds number around 4,000 and above. According to this, the critical Reynolds numbers were determined: 2,400 was the threshold for laminar and transition flows; whereas 4,000 was the threshold for transition and turbulence flows, of which two numbers are similar to those suggested in the literature (Munson et al., 2014). Therefore, as pre-designed experimental schedule, Reynolds number then was fixed at 2,400 and 4,000 to explore the flow regime impact on the selective transport of NH_3 by Hybrid Si PV membrane.

Additionally, this phenomenon confirmed the negative impact of temperature polarization on mass transfer in pervaporation. However, by introducing a more turbulent feed flow, this impact could be diminished to a certain degree (Favre, 2003). It should be noted that temperature of the feed solutions in this pure demi-water case was kept constant at 35 °C meaning the driving force was theoretically equal. Meanwhile, as has been assumed before, there was no concentration polarization in pure demi-water case. Therefore, based on these two assumptions, the difference in J_{H_2O} between laminar flow and turbulent flow can be rationally attributed to the temperature polarization effect. Temperature gradient (i.e. $T_i < T_f$) is well-developed in the boundary layer at laminar flow, which, as a consequence, the actual driving force over the membrane two sides is less than the theoretical driving force deduced from bulk solution (T_f). Karlsson et al. (1996), who studied the temperature polarization effect via a plate pervaporation membrane system fed with demi-water at 75 °C, found a temperature drop ($T_f - T_i$) of 1.1 °C when flow regime shifted from fully turbulent down to laminar. As a gross estimation, for this study, J_{H_2O} decreased by 23% meaning the temperature difference was about 3.3 °C (from 35 to 31.7 °C) if only driving force was affected regardless the temperature impact on solubility and diffusion coefficient inside the membrane.

4.2.2 Impact of Additional Salt

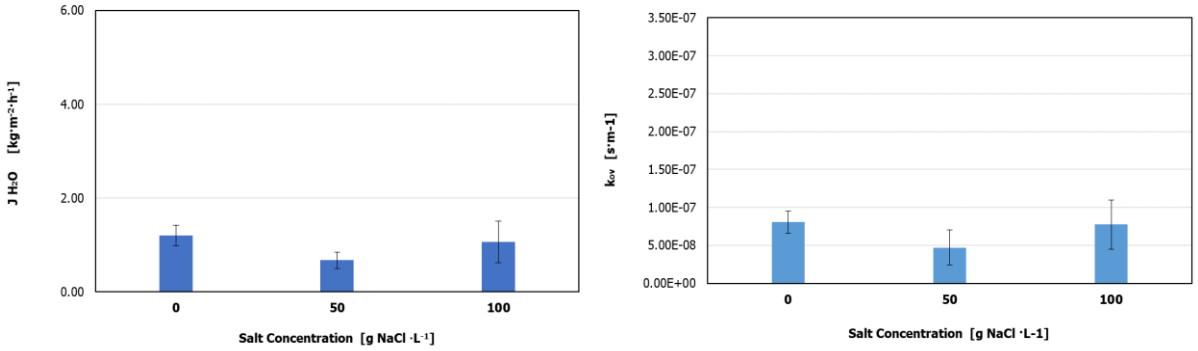

Figure 15 Results of salt case. a) Demi-water flux over different salt concentratitons; b) Overal mass transfer coefficient over different salt concentratitons. Error bars represent the standard deviation of samples taken in triplicate experiments.

Figure 15 displays the effect of the presence of salt (sodium chloride, $NaCl$) on the J_{H_2O} together with k_{ov,H_2O} of Hybrid Si PV membrane for H_2O transfer.

It can be seen that when the solution containing 50 g·L^{-1} of $NaCl$, J_{H_2O} and k_{ov,H_2O} presented one-third decrease compared to these without salt, which implied the presence of salt, at this level, not only negatively influenced the driving force but also adversely affected the behaviour of H_2O molecules inside the membrane matrix (i.e. mass transfer). Thus, as a result, the degree of drop observed was more significant than that caused by decrease of driving force, which merely around 5% (referring to Table 3).

Moreover, a more severe concentration polarization could be another reason for the decrease of k_{ov,H_2O}: boundary layer being more resistant to the movement of H_2O molecules. In general, results indicated it was k_{ov,H_2O} that determined J_{H_2O} in saline water tested rather than the driving force.

Nonetheless, it is also noteworthy that when the $NaCl$ concentration increased from 50 to 100 g·L^{-1}, J_{H_2O} exhibited an increasing trend that was opposite to the prediction regarding to the driving force. The same trend was also found in the result of k_{ov,H_2O}. Firstly, the driving force could not be the reason for this increase because it was lower in in saline solution than that in pure water solution. Secondly, the change in the boundary layer could not be the reason for this increase neither because the concentration polarization was more severe in saline solution than in pure water solution, which negatively impacted mass transfer. Hence, the cause of this phenomenon was highly associated with the change in the membrane layer, either by change of the solubility or the diffusivity or even both.

4.3 Impact of Flow Regime

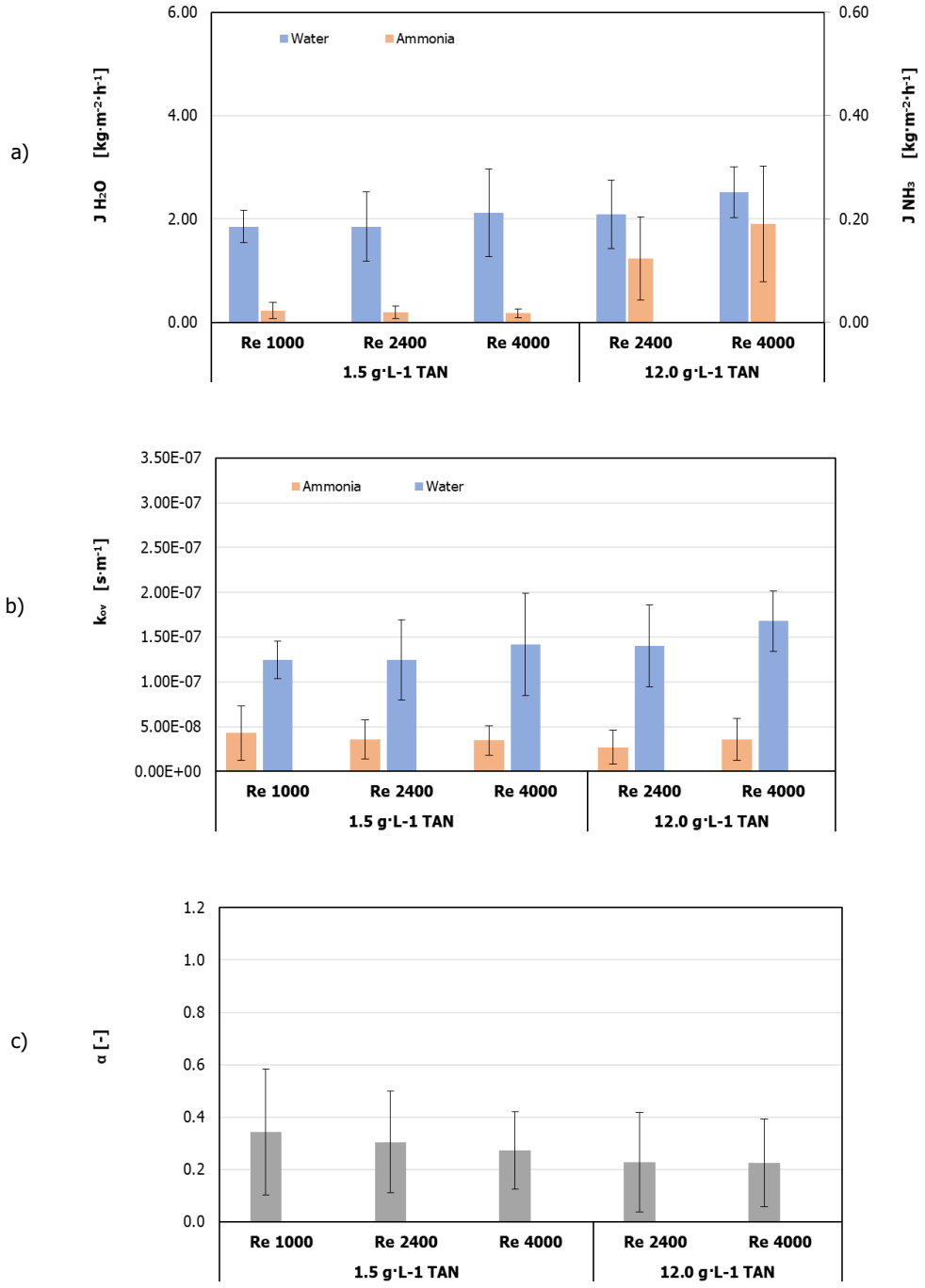

Figure 16 Results of AmmOH case: a) Flux over Reynolds number; b) Mass transfer coefficient over Reynolds number; c) Perm-selectivity over Reynolds number. Error bars represent the standard deviation of samples taken in triplicate experiments.

The impact of flow regime on the selective transport of NH_3 by Hybrid Si AR PV membrane was investigated in AmmOH case of which results are plotted in Figure 16.

Flux, J

Generally, for both J_{NH_3} and J_{H_2O}, the results were consistent with the hypothesis (Table 2): a turbulent flow regime positively affected the mass transfer. But interestingly, the degree of the influence was relating to the TAN content in the feed solution: it was more distinguishable in a higher TAN content.

For the 12.0 g TAN·L^{-1} AmmOH experiments, when flow regime shifted from laminar to fully turbulent, J_{NH_3} increased from 0.12 to 0.19 kg·m^{-2}·h^{-1} meanwhile J_{H_2O} increased from 2.09 to 2.52 kg·m^{2}·h^{-1}. This phenomenon confirms the finding (section 4.2.1) that the positive effect of turbulent flow regime on mass transfer was also applicable for ammonia-water binary system. Again, the increase of J_{H_2O} resulted from a reduced temperature polarization effect and so the actual driving force increased. As for NH_3 transfer, turbulent flow not only diminished the temperature polarization reducing the temperature gradient at the boundary layer but also diminished the concentration polarization effect reducing the concentration gradient simultaneously. Consequently, J_{NH_3} increased more than J_{H_2O}, being 50% comparing to 20%.

Contrary to the results of 12.0 g TAN·L^{-1} AmmOH experiments, the results of 1.5 g TAN·L^{-1} experiments were different from the hypothesis. Observations showed that though J_{H_2O} was positively related to the flow regime while J_{NH_3} was independent on the flow regime remaining at 0.02 kg·m^{-2}·h^{-1} approximately. This observation might be associated with three aspects.

- Less severe concentration polarization

  Comparing to 12.0 g TAN·L^{-1} experiment, at low TAN concentration, the concentration polarization effect for NH_3 was already minor making the change in J_{NH_3} less detectable even though the positive impact of turbulent flow regime had been proven to be true.

- Less severe temperature polarization

  As can be seen from (Figure 16 a.), the increase of J_{H_2O} for 1.5 g TAN·L^{-1} experiment was not as significant as that for 12.0 g TAN·L^{-1} experiment (14% vs 20%). Based on the assumption that the influence of concentration polarization on J_{H_2O} in AmmOH case was negligible, this moderate increase of J_{H_2O} suggested that the temperature polarization effect was also less severe when feed solution containing low TAN concertation than high. Therefore, the improvement of J_{NH_3} by reducing temperature polarization was limited.

  The degree of temperature polarization is related to heat loss which is associated with J_{total}. Accordingly, the existence of less severe concentration polarization in 1.5 g TAN·L^{-1} experiments can be explained by the smaller amount of heat loss due to a relatively low J_{total}. Notably, at each flow regime, compared with J_{total} of demi-water case, J_{total} (See Appendix) of this AmmOH case was much lower. Taking Re=4,000 for example, the total fluxes were 2.13 and 2.71 kg·m^{-2}·h^{-1}, respectively for 1.5 and 12.0 g TAN·L^{-1} experiments, both of which were lower than the flux of demi-water case (4.23 kg·m^{-2}·h^{-1}). Because of this low total flux, the amount of heat loss was less and so the temperature polarization. An evidence can also be found in the literature: temperature polarization effect is more influential in high flux pervaporation process (Khayet et al., 2004).

- Reduced k_{ov}

  According to the definition of J, it is determined not only by $(P_f - P_p)$, the driving force, but also by the k_{ov}. Apart from the driving force, shifting the flow regime was likely to negatively affect the mass transfer in the pervaporation process. Especially in 1.5 g TAN·L^{-1} experiments, reduced k_{ov} performed against the improvement by reducing polarization effects which were already limited in low TAN concentration solution. However, in 12.0 g TAN·L^{-1} experiments, the positive impact of flow regime was dominating and so increase of J_{NH_3} and J_{H_2O} were observed eventually.

Overall Mass transfer coefficient, k_{ov}

For the 12.0 g TAN·L^{-1} AmmOH experiments, k_{ov,H_2O} grew by 20%, from 1.40·10^{-7} to 1.68·10^{-7} s·m^{-1} stressing the important role of boundary layer resistance for H_2O transfer: the less the boundary layer resistance, the less the overall resistance to a certain degree. Similarly, k_{ov,NH_3} increased by 33% from 2.68·10^{-8} to 3.56·10^{-7} s·m^{-1}, which also resulted from a more turbulent flow regime.

A probable reason for a higher degree of increase observed for NH_3 than for H_2O was that, at laminar flow J_{NH_3} was not only restrained by temperature polarization but also concentration polarization effects (mostly the depletion of NH_3 at the boundary layer since there were no existing of additional salt); whereas J_{H_2O} was more restrained by temperature polarization. So that when the feed flow being more turbulent, the extent of reduced resistance of the boundary layer for NH_3 transfer became greater than that for H_2O transfer and eventually $\Delta k_{ov,NH_3} > \Delta k_{ov,H_2O}$.

However, for the 1.5 g TAN·L^{-1} experiments, k_{ov,NH_3} declined as the flow regime being more turbulent, being 4.28·10^{-8}, 3.59·10^{-8} and 3.44·10^{-8} s·m^{-1}, for laminar, transition and fully turbulent flow regime, respectively. This was opposite to the hypothesis. One interpretation being that with a limited space inside the membrane, NH_3 and H_2O molecules were competing with each other leading to a less efficient transportation. Camus et al. (2006), who tested the feasibility of pervaporation application on gas separation, also proposed this mutual competition between permeates: sorbed NH_3 molecules block pores preventing N_2 and H_2 entering the membrane structure.

In addition, shifting of dominated k was proposed to elaborate the opposite trends of k_{ov,NH_3} for both TAN experiments: at low TAN content, k_m dominated k_{ov}, whereas in high TAN content, k_f dominated. But to verify this hypothesis, further investigation was needed.

Perm-selectivity, α

In general, α of every experiment in the AmmOH case was less than one and the highest α, around 0.3, was found at the laminar flow regime and in lower NH_3 content solution, which was slightly less than that reported by Yang et al. (2016), 0.5, but the fact revealed was the same that H_2O was more selectively transported by Hybrid Si AR PV membrane instead of NH_3.

For the 12.0 g TAN·L^{-1} experiments, α remained approximately the same at 0.2. It was interesting to mention that when flow regime shifted from laminar to turbulent, k_{ov,NH_3} increased by 33% whereas k_{ov,H_2O} increased merely by 20%. This was reasonable because according to the values of k_{ov,NH_3} and k_{ov,H_2O}, α would increase by a factor of 1.1, from 0.2 to 0.22. However, based on the accuracy of calculation that only one digit was remained, 0.22 was round off to 0.2. Therefore, the same α were found. This phenomenon showed, though employing a more turbulent flow regime was more beneficial for NH_3 transfer, the extent of benefit was limited. H_2O was

selectively transported rather than NH_3. Due to the poor performance of selective transport of NH_3 by Hybrid Si AR PV membrane, changing the flow regime can hardly enhance the overall separation of NH_3 from liquid solution.

For the 1.5 g TAN·L^{-1} experiments, the results of α were consistent with the results of k_{ov}: as the flow regime being more turbulent, k_{ov,NH_3} decreased whereas k_{ov,H_2O} increased, which led to a decreasing trend of α. This suggested that Hybrid Si AR PV membrane presented a better performance in terms of NH_3 transport when the flow regime in the membrane tube was laminar. Moreover, from an energy-saving point of view, laminar flow was preferred.

4.4 Impact of Temperature

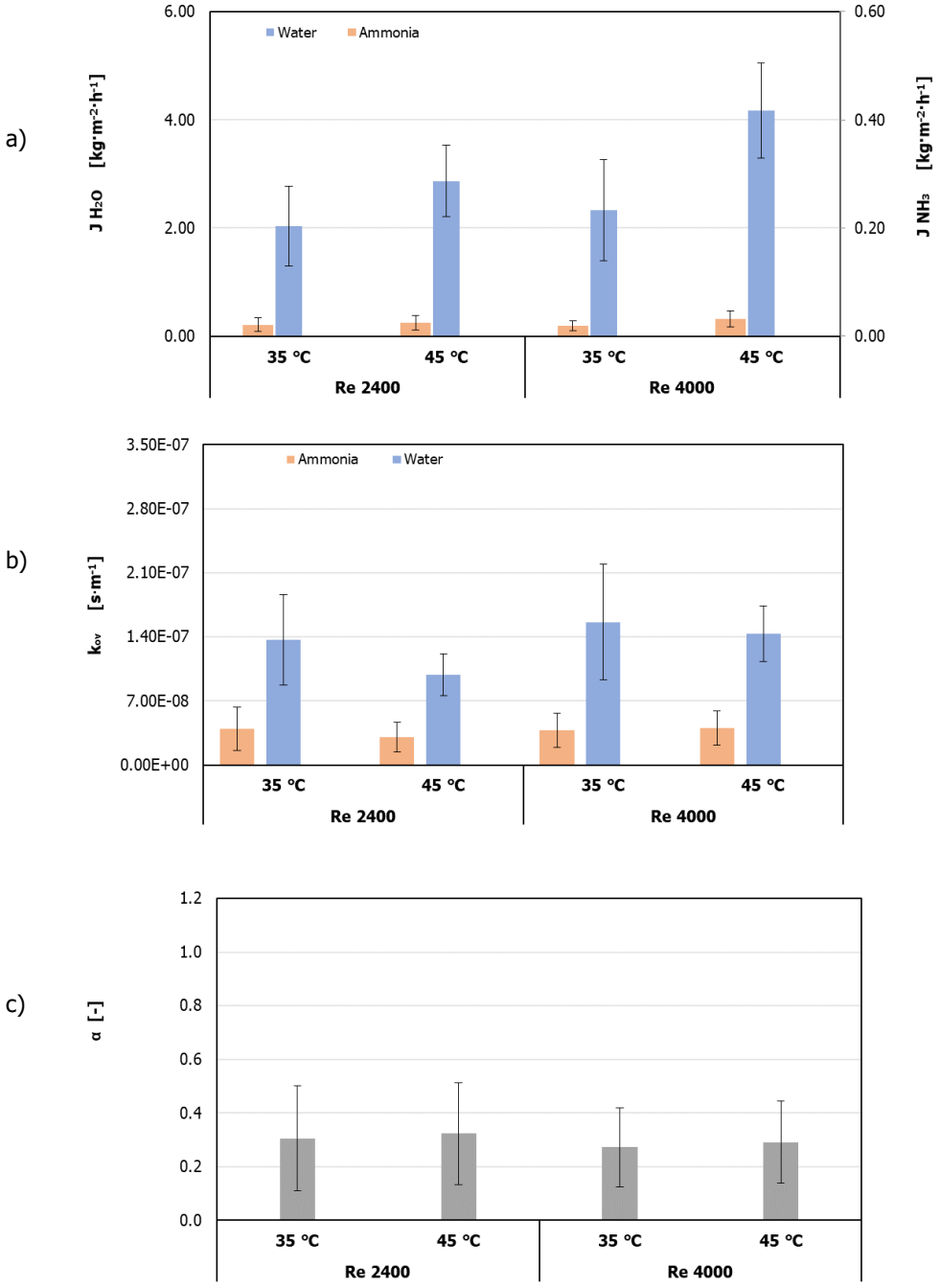

Figure 17 Results of AmmOH case: a) Flux over Temperature; b) Mass transfer coefficient over Temperature; c) Perm-selectivity over temperature. Error bars represent the standard deviation of samples taken in triplicate experiments.

The impact of temperature (35 and 45 °C) on the selective transport of NH_3 by Hybrid Si AR PV membrane was investigated in AmmOH case (1.5 g TAN·L^{-1}) of which the results are plotted in Figure 17.

Flux, J

As expected, both J_{NH_3} and J_{H_2O} increased as temperature increasing which agreed with the hypothesis.

In turbulent flow regime (i.e., Re=4,000), J_{NH_3} increased by a factor of 1.6, which was less than J_{H_2O} (1.8). This difference between both species could be partially ascribed to the different degree of enhanced driving force: according to the PHREEQC simulation, P_{f,NH_3} and P_{f,H_2O} had increased by a percent of 53% and 70%, respectively, when temperature rose from 35 to 45 °C. Small discrepancy between simulation and experiment outcomes were likely because of the fluctuation of partial pressure at the membrane permeate side (discussed in section 4.8).

In laminar flow regime (i.e., Re=2,400), J_{NH_3} stayed the same at 0.02 kg·m^{-2}·h^{-1} whereas J_{H_2O} presented the same upward trend than that in turbulent flow regime but rather mild. It was reasonable because, as afore-verified, temperature polarization effect was more sever in a laminar flow regime (section 4.2.1), the increase of J_{H_2O} was restrained somehow by this effect although the theoretical driven force increased to the same extent.

Overall Mass transfer coefficient, k_{ov}

In turbulent flow regime, k_{ov,NH_3} remained almost the same at 4.00 ·10^{-8} s·m^{-1} and k_{ov,H_2O} fluctuated around 1.40 ·10^{-7} s·m^{-1}. This stable k_{ov} suggests that the impact of temperature on pervaporation process, in this flow regime, might mainly lay on driving force instead of on k_{ov}.

Notably, in laminar flow regime, k_{ov,NH_3} instead of remaining the same, decreased from 3.95 ·10^{-8} to 3.05 ·10^{-8} s·m^{-1}, which was the same for k_{ov,H_2O}, that decreased from 1.37 ·10^{-7} to 0.99 ·10^{-7} s·m^{-1}. This phenomenon might relate to the resistance at different layers.

- Reduced k_f

  On the hand, the temperature polarization was more significant at 45 °C than at 35 °C due to a higher J_{total}. On the other hand, the depletion type of concentration polarization was more significant at a higher temperature due to a higher J_{NH_3}. Both polarization effects increased the resistance at the boundary layer reducing k_{f,NH_3}.

- Reduced k_m

  There was a likelihood that increasing temperature of the feed solution hindered NH_3 transfer in the membrane structure (i.e., k_{m,NH_3}) (Cheng et al., 2017). It could be, in this flow regime, a higher temperature reduced either the solubility of NH_3 in hybrid Si or the diffusion of NH_3 in membrane matrix or both, and together with the intensified polarisation effects in the boundary layer caused a decrease of k_{ov,NH_3}.

As for k_{ov,H_2O}, except the concentration polarization, temperature polarization and the possible change in k_{m,H_2O} could explain its decrease.

Perm-selectivity, α

In general, α in laminar flow regime was higher than that in turbulent flow regime which was in accordance with the founding in section 4.3 that laminar flow regime was preferred for selective transport of NH_3. However, as plotted in Figure 17 c, at the same flow regime, α stayed the same level, though both k_{ov,NH_3} and k_{ov,H_2O} were negatively affected by the increase of temperature. This phenomenon suggested that there was no apparent relationship between α and temperature in the temperature range of 35 to 45 °C. But it was worth noting that in laminar flow, the enhanced temperature polarization and possible change in k_m due to the increase of temperature would have negative impact on both NH_3 transfer and H_2O transfer.

On the one hand, the independence of α on temperature showed that the membrane used in this study was thermal-resistant within the temperature range tested; on the other hand, it also implied the intrinsic affinity of Hybrid Si towards ammonia was not sensible to temperature. In other words, it is ineffective to improve the selective transport of NH_3 by means of adjusting the temperature as least in the range of 35 to 45 °C.

Concerning energy consumption of the entire system a lower operation temperature was recommended when using Hybrid Si AR PV membrane for selective transport of NH_3. Besides, according to the results and the scheduled research plan, the temperature of feed solutions for the rest experiments were remained at 35 °C.

4.5 Impact of TAN Concentration

a)

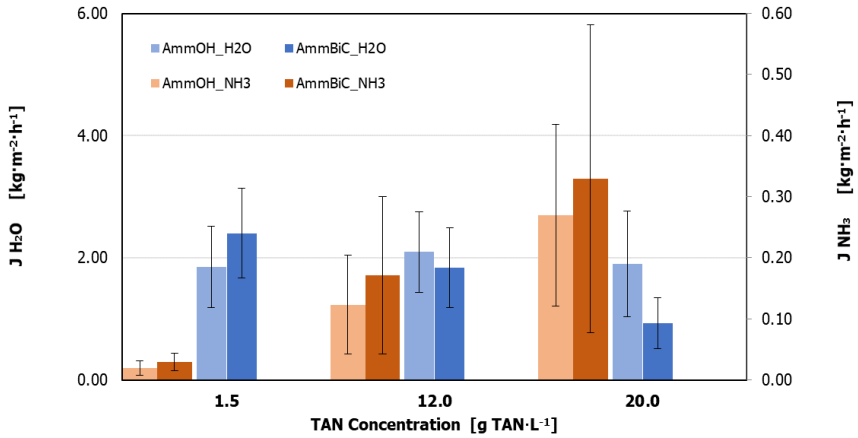

b)

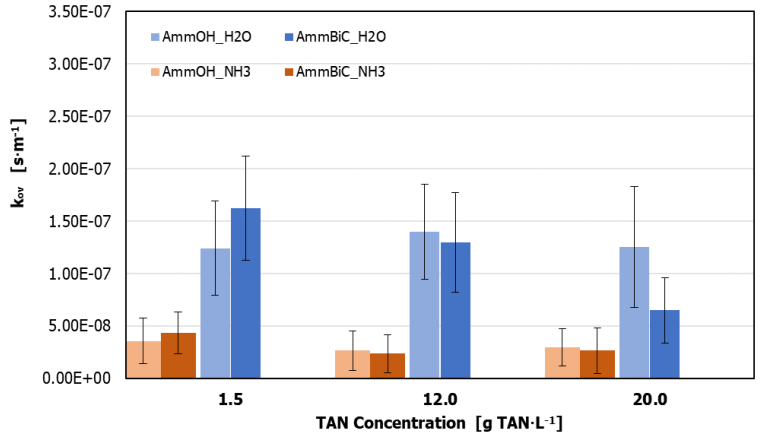

c)

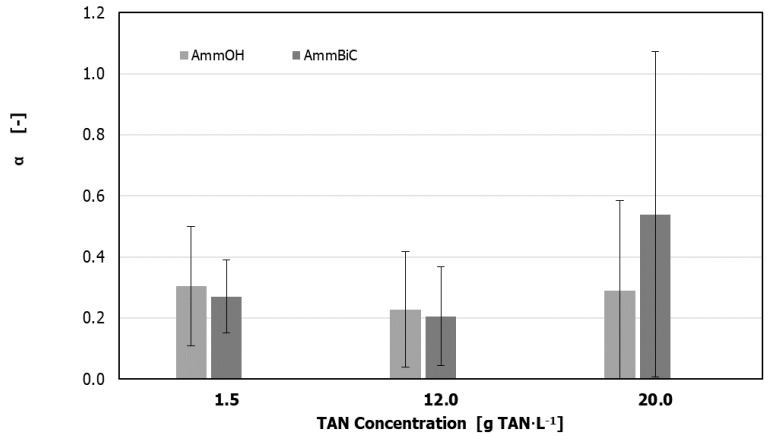

Figure 18 Results of AmmOH and AmmBiC cases regarding TAN concentration and the presence of additional salt: a) Flux; b) Mass transfer coefficient of water and amonia; c) Perm-selectivity. Error bars represent the standard deviation of samples taken in triplicate experiments.

The impact of TAN concentration on the selective transport of NH_3 by Hybrid Si AR PV membrane was investigated in AmmOH case of which results are plotted in Figure 18.

Flux, J

In general, J_{NH_3} presented an increasing trend, rising from 0.02 to 0.17 and to 0.27 kg·m^{-2}·h^{-1} for 1.5, 12.0, and 20.0 g TAN·L^{-1} respectively, which was in line with the hypothesis.

It was worth noting that the degree of the increase of J_{NH_3} was almost the same as that of the increase of the driving force of NH_3, for instance, by a factor of 12 for both J_{NH_3} and driving force when the TAN concentration in the feed solution increased from 1.5 to 20.0 g·L^{-1}. This showed that the TAN concentration influenced J_{NH_3} mainly by influencing the driving force of NH_3.

In contrast to J_{NH_3} , J_{H_2O} in this case were relatively stable at 2.00 kg·m^{-2}·h^{-1} showing its independence on TAN concentration which was also line with the hypothesis. This was reasonable since the driving force of H_2O was almost equal for each experiment (see Table 3).

Overall Mass transfer coefficient, k_{ov}

Unlike J_{NH_3}, k_{ov,NH_3} remained almost stable with slight fluctuation, being 3.59·10^{-8}, 2.68·10^{-8} and 2.97·10^{-8} s·m^{-1}, respecting to the three TAN concentration points. This further confirmed that the increase of J_{NH_3} was primarily associates with the enhanced driving force. As for the variation of k_{ov,NH_3}, it could be attributed to two possible reasons.

- Change in k_m

  On the one hand, the increased J_{NH_3} could lead to a more severe depletion of NH_3 at the boundary layer, which was negative for NH_3 transfer. On the other hand, it should be noted that the TAN concentration in the feed solution was increasing as well, which might compensate the loss of NH_3 at the boundary layer to a certain degree. The contradicting effects might cause a fluctuation of the resistance at the boundary condition but need further investigation.

- Change in k_f

  Another reason could be the change in membrane layer (mainly the diffusion coefficient). Camus et al. (2006) who observed a similar influence of NH_3 concentration on k_{ov,NH_3} using zeolite ceramic PV membrane claimed that it is due to a change of governing transport mechanism (which they did not point out) as NH_3 being more saturated in the feed-membrane interface.

As expected, k_{ov,H_2O} was basically staying the same in the TAN concentration range of 1.5 to 20 g·L^{-1} meaning, in general, k_{ov,H_2O} was independent on the TAN concentration. A small variation could be related to the increased resistance in the boundary layer for H_2O transfer due to the presence of increasing amount of NH_3 molecules.

Perm-selectivity, α

It can be seen from Figure 18 c, α kept almost the same at 0.3 meaning α was almost independent on the TAN concentration. In other words, transport of H_2O and NH_3 by Hybrid Si PV membrane, to a certain degreed, were equally affected by TAN concentration.

When increasing the TAN concentration in the feed solution although J_{NH_3} was increasing indicating more NH_3 can be obtained per unit of time, the ability of Hybrid Si PV membrane on selective transport of NH_3 was not

improved since k_{ov,NH_3} remained the same. The influence of TAN concentration was similar to the influence of temperature (discussed in 4.4), both of which mainly affected the driving force of NH_3 instead of affecting the ability of Hybrid Si on NH_3 transport.

The different role of concentration polarization effect played in NH_3 and H_2O transfer might explain the small variation of α. The depletion type of concentration polarization would affect NH_3 transfer but would not affect H_2O; while H_2O transfer might be hindered by the increased resistance due to the presence of more NH_3 molecules at the boundary layer. Nonetheless, TAN concentration was not able to improve the ability of hybrid Si PV membrane for selective transport of NH_3.

4.6 Impact of Additional Salt

The impact of presence of salt on the on the selective transport of NH_3 by Hybrid Si AR PV membrane was investigated in AmmBiC case of which results are plotted in Figure 18.

Flux, J

It can be seen in Figure 18 a., for the tested three TAN concentrations, J_{NH_3} was benefited from the presence of salt as it was higher than that of experiment without salt whereas J_{H_2O} was not except the 1.5 g TAN·L^{-1} experiment.

The increase of J_{NH_3} was associated with the salting-out effect which directly increased P_{f,NH_3}. Because less NH_3 was dissolved in the liquid solution, more NH_3 was free to be transported through the membrane matrix (i.e., the activity of NH_3 increases). This results also confirmed the results of the PHREEQC simulation that the salting-out effect was stronger than the ionization of NH_3 (as discussed in 2.5.3).

The increase of J_{H_2O} observed in 1.5 g TAN·L^{-1} experiment might be explained by the electrostatic-shielding effect. Lipnizki et al. (2004) stated that the water shell of inorganic ions in aqueous solution increases the affinity between these ions and the membrane material if it is hydrophilic with the evidence that inorganic ions were observed on their feed-membrane interface and also inside the membrane structure. If it was so, in this research, the measured weight difference (Δm_i) would be larger than the actual change of permeates since J was determined based on the change of feed solution in weight. Consequently, the mass of hydrates was included, which was apparently inappropriate. However, it was an arbitrary explanation since the hydrates were by no means able to penetrate into the membrane matrix according to size sieving mechanism.

As for the decrease of J_{H_2O} observed in 12.0 and 20.0 g TAN·L^{-1} experiments, it might be explained by two reasons:

- Concentration Polarization

  Since salt is impermeable, it would be retained by the membrane and further accumulated at the boundary layer. Hence, the accumulation type of concentration polarization was intensified providing an extra resistance for H_2O transfer, which led to a lower J_{H_2O}.

- Membrane Fouling

  For the 20.0 g TAN·L^{-1} experiment where salt was present, J_{H_2O} reduces by 50%. Besides the

negative impact of concentration polarization, membrane fouling might be an additional reason for this significant decrease. Evidence can be found in the literature that Lipnizki et al.(2004) claimed: importable ions partially block the membrane surface leading to a decrease of mass flux. To verify this phenomenon, autopsy analysis should be performed.

Overall Mass transfer coefficient, k_{ov}

As shown in Figure 18 b., for each TAN concentration, k_{ov,NH_3} stayed at the same level no matter there was salt or not in the feed solution (AmmBiC case vs AmmOH case). Combining this result and that of J_{NH_3} it can be seen that the impact of presence of salt for NH_3 transfer could be attribute to the driving force to a large extent since J_{NH_3} increasing while k_{ov,NH_3} remaining approximately the same as AmmOH case.

In terms of k_{ov,H_2O}, the results showed that salt influenced the behaviour of H_2O molecules (i.e. diffusivity or solubility) inside the membrane matrix since k_{ov,H_2O} reduced except for the 1.5 g TAN·L^{-1} experiment, which agreed with the explanation for the decrease of J_{H_2O}. Lipnizki et al. (1999) considered the change in k_{ov,H_2O} as a result of coupled diffusion which was basically in line with Camus et al. (2006) who announced a competition between molecules: the diffusion of one permeate can be changed by the presence or movement of other penetrates. For this study, competitions exist among H_2O and NH_3 or even unexpected penetrated sodium hydrates.

Perm-selectivity, α

The results of α were almost the same as the results when there was no presence of salt except the 20.0 g TAN·L^{-1} experiment where α of AmmOH and AmmBiC cases were 0.5 and 0.3, respectively. Moreover, the former one (0.5) was the highest α observed among all case studies.

Although the presence of salt did not show significant influence on the selective transport of NH_3 by Hybrid Si AR PV membrane, it decreased the selective transport of H_2O, which resulted in an enhanced separation of NH_3 from liquid solution. Besides the influence of the salt on the driving force of H_2O which had been proven to be limited by PHREEQC simulation, the influence of the salt on k_{ov,H_2O} was more significant. Both k_{f,H_2O} and $k_{m,,H_2O}$ could be affected that caused a change in k_{ov,H_2O}, but due to the knowledge gap discussed in 2.3, quantifying the two k was still a challenge and should be stressed in the further study.

Additionally, it should be noted that although the highest α was still less than unity, it was a positive sign that the Hybrid Si AR PV membrane might probably be able to operate in highly saline environment because the concentration of salt (Na_2CO_3 after pH adjustment) already exceeded 100 g·L^{-1} being 120 g·L^{-1} in fact.

Finally, the drastic influence of the presence of salt on α might suggested that introducing additional ions in the membrane material might be a promising approach for enhancing the selective transport of NH_3.

4.7 Energy Consumption

Table 5 Results of energy balance of lab-scal ammonia pervaporation process

TAN Concentration	Average J_{NH_3}		Thermal Heat, $\Delta H'_{i,NH_3}$		
	AmmOH	AmmBiC	AmmOH	AmmBiC	SOFC[a]
[g TAN·L^{-1}]	[kg·m^{-2}·h^{-1}]		[MJ·kg^{-1} -N]		
1.5	0.02	0.03	192	167	
12.0	0.12	0.17	36	23	6.5
20.0	0.27	0.33	16	7	

[a] Thermal heat produced by SOFC. According to Stambouli et al. (2002) assumed a 50% of electrical generation efficiency and 35% of thermal energy generation efficiency.

Table 5 shows the energy that was consumed by the lab-scale NH_3 pervaporation processes and that can be produced by the lab-scale ammonia-fueled SOFC. In general, at current stage, NH_3 pervaporation-cracking cycle was still energy negative and the total energy demand of the system was inversely proportional to TAN concentrations.

In terms of thermal energy, the AmmBiC required less than the AmmOH case in all TAN levels, both of which the energy consumption decreased exponentially as TAN concentration went up. This finding agreed with the results presented in Figure 18 a. in which, J_{NH_3} was proportional to the TAN concentration whereas J_{H_2O} was not. Hence, the portion of useful energy demand (to change the phase of NH_3 instead of H_2O) rose making the utility of thermal energy more efficient. As suggested by this decreasing trend of heat consumption, the likelihood of achieving an energy-positive NH_3 pervaporation system was still high as long as TAN in the feed solution was concentrated enough, like some industrial wastewater or concentrated urine.

Table 6 Comparison of energy consumption for treating NH_3 by various technologies and energy production of NH_3 - fueled SOFC

Energy Production	Energy Consumption		
SOFC[a]	Air stripping[b,c]	Anammox[b]	Pervaporation
[MJ·kg^{-1} -N]		[MJ·kg^{-1} -N]	
14	50	19	167[d]; 7[e]

[a] Including thermal and electrical energy (Dekker et al., 2006).
[b] Data based on 2.8 g TAN·L^{-1} solution and excluding energy demand for building materials and devices (Magrí et al., , 2013).
[c] Digester supernatant treatment by air stripping for heating and production of $(NH_4)_2SO_4$ (Magrí et al., , 2013).
[d] Thermal energy demand for AmmBiC 1.5 g TAN·L^{-1} case.
[e] Thermal energy demand for AmmBiC 20.0 g TAN·L^{-1} case.

A comparison made among the air stripping, Anammox and pervaporation in terms of N treatment or recovery indicated that at a low TAN content, conventional technology was still more energy-efficient for N removal. It was rational, as indicated in Eq. 45 and by plotting the data in Table 5, the energy consumption would be infinitely high if PV was applied for N treatment or recovery purpose when TAN concentration in raw water was very low. However, as the raw water being more TAN-concentrated, the advantage of using PV was apparent especially when the salinity in the raw water was high at the same time (discussed in 4.5.2)

4.8 Concentration Factor

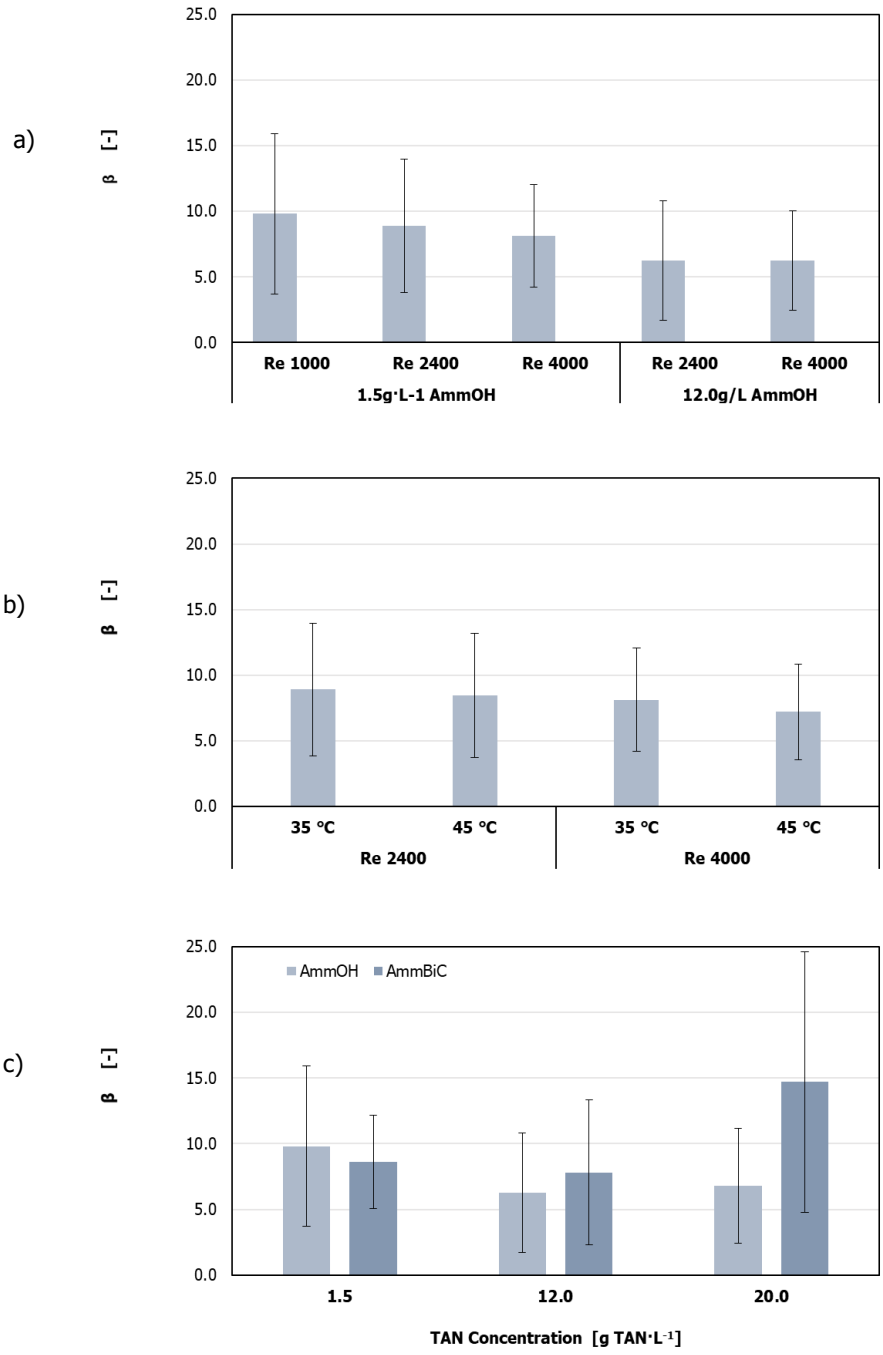

Figure 19 Concentration factor of each experimental conditiona. a) Concentration factor over Reynolds number; b) Concentration factor over temperature;c) Concentration factor over TAN concentration and presence of additional salt. Error bars represent the standard deviation of samples taken in triplicate experiments.

Figure 19 shows β of each experiment. It could be seen clearly that β did not exceed 33 as expected when 1.5 g TAN·L^{-1} was feed under various operation conditions.

The results were similar to α, which indicated that selective transport of NH_3 by Hybrid Si PV membrane was restrained by k_{ov,NH_3}. Because, for example, if the driving force was more dominated than k_{ov}, as the TAN concentration increasing (i.e. the diving force increasing), a higher β should be observed. However, in practical, β remained approximately the same. More detailed discussion can be seen in previous sections.

4.9 Data Deviation

Experimental results exhibited rather significant deviation which was abnormal compared with data presented in the literature even when the similar hybrid Si AR PV membrane was studied (Yang et al., 2016). This significant data deviation led to less reliable conclusions occasionally. In fact, during almost every experiment in AmmOH and AmmBiC cases, negative J_{NH_3} (i.e. reversed flux) was observed. Apart from systematic error from instrument or measurement, fluctuation of the driving force was considered with high likelihood as explained below:

Giving two consecutive time slots (T_n and T_{n+1}), supposing J_{NH_3} was remarkably higher than water flux during T_n resulting in a rather NH_3 concentrated permeate. If this part of permeate cannot be swept away rapidly enough, it might condense nearby, for example, the wall of membrane housing. Consequently, the condensate drops increased the partial pressure of NH_3 at the permeate side and consequently fluctuates the driving force. So, a reduced J_{NH_3} would be detected in the later time slot (i.e. T_{n+1}). As the driving force shifting, increasing or decreasing J_{NH_3} occurred periodically over time.

Noticeably, in Figure 17 a. AmmOH case, the error bar of J_{NH_3} of 1.5 g TAN·L^{-1} solution was relatively small which might be because of its relatively lower concentration making the fluctuation less detectable; while, as the TAN concentration increased, the data deviation became more significant. However, from a partial pressure point of view, for 20.0 g TAN·L^{-1} solutions, 35 °C, P_{f,NH_3} was about 3,000 Pa (Table 3) which was by no means exceeded by P_{p,NH_3} (maximum 1,500 Pa) no matter how concentrated NH_3 was in the permeate. This suggestted a reversed flow was theoretically impossible in this situation but was observed in practice.

Osmotic pressure might be considered as another plausible explanation, which has been reported in DCMD (direct contact membrane distillation) literature (Findley, 1967; Lawson et al, 1997). Lawson et al. (1997) claimed that in DCMD, if the permeate presents a higher osmotic pressure than the feed, permeate tends to transfer back to the feed solution; a positive J can be observed only when this osmotic pressure difference is overcome. If there were indeed liquid existing at the permeate side, this interpretation might also be applicable. Even though, this explanation was inconvincible for AmmBiC case, especially for 20.0 g TAN·L^{-1} solution, in which, the osmotic pressure of the feed solution was higher because of the existence of salt.

Nevertheless, this driving force dynamic was scarcely reported in pervaporation literature, which probably because of a relatively high sampling frequency (every 15-20 min) in this research comparing with 30 min or longer that was usually seen in the literature (Yang et al., 2016; You at al., 2014). This high sampling frequency made more detailed information attenable. That was a dynamic mass transfer during pervaporation process.

5 Conclusion

In this research, the selective transport of NH_3 by silica-based ceramic pervaporation membrane was investigated by studying the influences of various operational parameters on NH_3 transport in hydrophobic PDMS and hydrophilic Hybrid Si AR pervaporation membranes. It was found that PDMS PV membrane selected was not suitable for experiment due to its poor stability when exposed to solutions used in this study. Main conclusions were drawn based on the results of Hybrid Si AR PV membrane by answering each research questions as follows.

1. What is the optimum operating condition?

Among the tested conditions, the optimum condition for selective transport of NH_3 was 35 °C, Re=2,400, 20 g TAN·L^{-1} in the feed solution, at which condition the α was 0.5.

1.a What is the impact of flow regime on the flux, MTC and perm-selectivity?

The impact of flow regime on NH_3 transport by Hybrid Si AR PV membrane was associated with polarization effects but depended on the TAN content in the feed solution.

In a high TAN content, J and k_{ov} increased as the flow regime being more turbulent for both H_2O and NH_3. However, α was independent on flow regime. In a low TAN content, a more turbulent flow regime was positive for J_{H_2O} and k_{ov,H_2O} but negative for $k_{ov,NH_3}$and irrelated to J_{NH_3}. Concenquently, α was negatively related to flow regime.

1.b What is the impact of temperature on the flux, MTC and perm-selectivity?

The impact of temperature on the selective transport of NH_3 by hybrid Si PV membrane was mainly due to P_f and so the driving force. Moreover, J_{H_2O} benefitted more than J_{NH_3}. In the range of 35 °C to 45 °C, α was independent on temperature because both k_{ov,NH_3} and k_{ov,H_2O} were affected to a relatively the same extent.

1.c What is the impact of feed TAN concentration on the flux, MTC and perm-selectivity?

The impact of TAN content on the selective transport of NH_3 by hybrid Si AR PV membrane was mainly due to P_f so the driving force. Moreover, J_{NH_3} benefitted more than J_{H_2O}. In the TAN concentration range of 1.5 to 20.0 g·L^{-1} (AmmOH), α was independent on TAN concentration since k_{ov,H_2O} and k_{ov,NH_3} were basically not affected by the TAN concentration.

1.d What is the impact of additional salt on the flux, MTC and perm-selectivity?

The presence of salt positively affected the selective transport of NH_3. k_{ov,NH_3} was basically not affected by the presence of salt but k_{ov,H_2O} was negatively affected. Therefore, the presence of sat was beneficial for α. Additionally, salting-out effect played an important role in selective transport process of NH_3.

2. How much energy is consumed per unit of permeated ammonia at the optimum operating condition?

Energy consumed by transporting NH_3 was 7 MJ·kg^{-1} -N. The energy consumption decreased exponentially as TAN content increasing. For NH_3 recovery purpose, compared with air stripping, pervaporation was more energy-efficient when the raw water is more TAN-concentrated and saline.

6 Recommendation

As pointed out in section 2.3, a comprehensive understanding of the mass transfer in the boundary layer was impeded by the incompleteness of Sherwood and Nusselt correlations. In the future, research on pervaporation could target at this limitation by integrating mass and heat transfer together with descriptions of concentration polarization and temperature polarization effects.

Besides the theoretical part, "to test the feasibility of selective transport of NH_3 by metal-doped pervaporation membrane material" could also be a research objective of great potential. In the literature, research on pervaporation membrane doped with transition metal like iron and cobalt has been conducted occasionally with the purpose of increasing the affinity towards target species or the performance stability of membrane per se (Cheng et al., 2017; Yang et al., 2014, 2018). Especially for the affinity to ammonia, copper could be a promising transition metal to be doped in the membrane material, giving two reasons:

- A phenomenon observed by coincidence during experiments

  The blue solution shown in Figure 20 a). was the solution of the first experiment using NH_4HCO_3 solution (pH=10, AmmBiC case). An initial suspect to this phenomenon was the presence of Copper (Cu) originating from the endcaps of membrane housing (shown in Figure 20 b) which was made of brass (a type of alloy usually consisting of copper, zinc and cadmium). Through a desk research, this perspective was verified (Uhlig, 1948). It was found that this blue colour was due to the formation of a positively charged complex of NH_3 and Cu^{2+}, called tetraamminediaquacopper (II) which has a octahedral shape as shown in Figure 21 (Trevani et al., 2001).

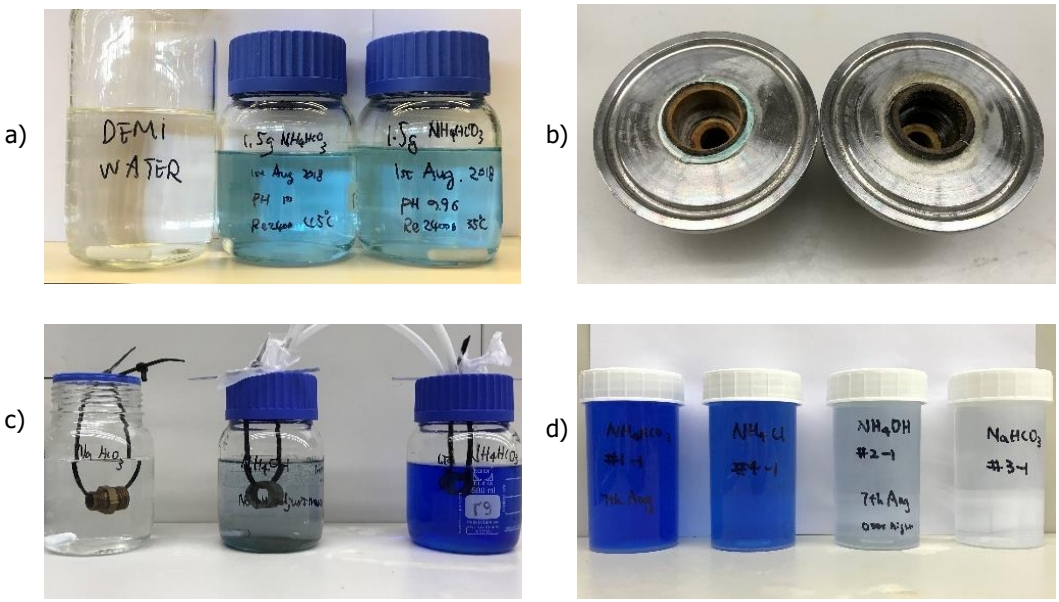

Figure 20 a) Appearance of blue in the feed solution compared with transparent pure water (1 hour experimental duration); b) Endcaps of the membrane housing; c) Brass pipe connections immersed in $NaHCO_3$, NH_4OH, and NH_4HCO_3 solutions from left to right for 17 hrs ; d) From left to right: final solutions with NH_4HCO_3, NH_4Cl, NH_4OH and $NaHCO_3$, respectively, (17 hrs of experimental duration).

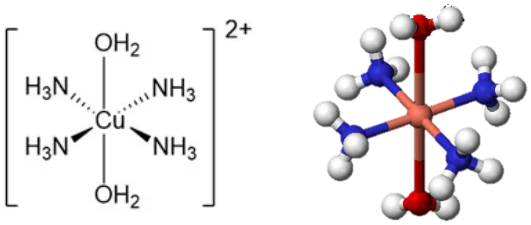

Figure 21 Tetraamminediaquacopper complex and its ball and stick model.

A series of controlled experiments (pH of all initial solution was adjusted to 10 except NH_4OH; Figure 20 c. and d.), indicated in alkaline environment, the blue colour would only be observed at the presence of both NH_3 and Cu^{2+}. Moreover, it was more visible by the presence of $CO_3^{2-}$and Cl^- compared to that of OH^-, which might be related to the solubility.

Eq. 46 shows that once Cu is dissolved as Cu^{2+}, it will react with NH_3. The high K° suggests this reaction will happen immediately, which indicates a strong affinity between NH_3 and Cu.

$$[Cu(H_2O)_6]^{2+}_{(aq)} + 4NH_{3_{(aq)}} \rightleftharpoons [Cu(NH_3)_4(H_2O)_2]^{2+}_{(aq)} + 4H_2O_{(l)} \qquad \textit{Eq. 46}$$

$K^\circ = 1 \cdot 10^{13}$ (Miessler et al., 2014)

- Facilitated mass transfer mechanism

Besides the sorption-diffusion mechanism, a group of academic also support the facilitated transfer mechanism (Cheng et al., 2017). This mechanism stresses a reversible chemical reaction between target molecules and membrane material so that the membrane material serves as a conveyor to accelerate the transport of target molecules in addition to the traditional sorption-diffusion. Perm-selectivity is then subject to the speed of the reverse reaction (Shao et al., 2007).

The key difference between sorption-diffusion and facilitated transfer mechanisms is whether there is a reversible chemical reaction between membrane material and penetrated molecules. Notably, the reaction between NH_3 and Cu^{2+} (Eq. 41) is reversible. Accordingly, if Cu is doped into a PV membrane, at the feed-membrane interface, where NH_3 is abundant, so as the reaction shifting to the right (Eq. 46), NH_3 is selectively bound. Meanwhile, at the permeate-membrane interface, the reaction shifts to the left since NH_3 is depleted (sucked away a by vacuum pump).

Considering these two factors, Cu was therefore recommended to be doped into the material of PV membrane for the application of selective transport of NH_3, of which the feasibility requires further study.

Reference

Ahmad, S. A., & Lone, S. R. (2012). Hybrid Process (Pervaporation-Distillation): A Review. *International Journal of Scientific & Engineering Research*, *3*(5), 1–5.

Anthonisen, A. C., Loehr, R. C., Prakasam, T. B. S., & Srinath, E. G. (1976). Inhibition of nitrification by ammonia and nitrous acid. *Journal (Water Pollution Control Federation)*, 835–852.

Appelo, C. A. J., & Postma, D. (2004). *Geochemistry, groundwater and pollution* (2nd ed.). CRC press.

Beck, M. B., & Speers, A. (2006). *2nd IWA Leading-Edge on Sustainability in Water-Limited Environments*. IWA Publishing.

Bergman, T. L., Lavine, A. S., Incropera, F. P., & Dewitt, D. P. (2011). *Fundamentals of Heat and Mass Transfer*. John Wiley & Sons.

Böddeker, K. W. (1990). Terminology in pervaporation. *Journal of Membrane Science*, *51*(3), 259–272. https://doi.org/10.1016/S0376-7388(00)80350-6

Camus, O., Perera, S., Crittenden, B., van Delft, Y. C., Meyer, D. F., & Pex, P. A. C. (2006). Ceramic Membranes for Ammonia Recovery. *AIChE Journal*, *52*(6), 2055–2065. https://doi.org/10.1002/aic

Cheng, X., Pan, F., Wang, M., Li, W., Song, Y., Liu, G., … Jiang, Z. (2017). Hybrid membranes for pervaporation separations. *Journal of Membrane Science*, *541*(July), 329–346. https://doi.org/10.1016/j.memsci.2017.07.009

Dekker, N. J. J., & Rietveld, G. (2006). Highly Efficient Conversion of Ammonia in Electricity by Solid Oxide Fuel Cells. *Journal of Fuel Cell Science and Technology*, *3*(4), 499. https://doi.org/10.1115/1.2349536

EDI. (2011). EDI:Aeration Efficiency Guide. Retrieved from http://www.wastewater.com/docs/default-source/corporate/aeration-efficiency-guide.pdf?sfvrsn=b905df4f_4

El-Bourawi, M. S., Ding, Z., Ma, R., & Khayet, M. (2006). A framework for better understanding membrane distillation separation process. *Journal of Membrane Science*, *285*(1–2), 4–29. https://doi.org/10.1016/j.memsci.2006.08.002

Favre, E. (2003). Temperature polarization in pervaporation. *Desalination*, *154*(2), 129–138. https://doi.org/10.1016/S0011-9164(03)80013-9

Feng, X., & Huang, R. Y. M. (1997). Liquid Separation by Membrane Pervaporation: A Review. *Industrial and Engineering Chemistry Research*, *36*(4), 1048–1066. https://doi.org/10.1021/ie960189g

Findley, M. E. (1967). Vaporization through porous membranes. *Industrial and Engineering Chemistry Process Design and Development*, *6*(2), 226–230. https://doi.org/10.1021/i260022a013

Frank, M. J. W., Kuipers, J. A. M., & van Swaaij, W. P. M. (1996). Diffusion Coefficients and Viscosities of CO2 + H2O, CO2 + CH3OH, NH3+H2O, and NH3+ CH3OH Liquid Mixtures. *Journal of Chemical & Engineering Data*, *41*(2), 297–302. https://doi.org/10.1021/je950157k

Giddey, S., Badwal, S. P. S., Munnings, C., & Dolan, M. (2017). Ammonia as a Renewable Energy Transportation Media. *ACS Sustainable Chemistry and Engineering*, *5*(11), 10231–10239. https://doi.org/10.1021/acssuschemeng.7b02219

Guerrini, A., Romano, G., & Indipendenza, A. (2017). Energy efficiency drivers in wastewater treatment plants: A double bootstrap DEA analysis. *Sustainability (Switzerland)*, *9*(7), 1–13. https://doi.org/10.3390/su9071126

Heintz, A., & Stephan, W. (1994). A generalized solution-diffusion model of the pervaporation process through composite membranes Part II . Concentration polarization , coupled diffusion and the influence of the porous support layer DiM = ;;; f : sjF. *Journal of Membrane Science*, *89*(93), 153–169.

Helgeson, H. C. (1967). Thermodynamics of complex dissociation in aqueous solution at elevated temperatures. *The Journal of Physical Chemistry*, *71*(10), 3121–3136.

Hendricks, D. (2006). *Water treatment unit processes: physical and chemical*. CRC press.

Hirabayashi, Y. (2002). Pervaporation Membrane System for the Removal of Ammonia from Water. *Material*

Transaction, *43*(5), 1074–1077.

Holley Jr, C. E., Worlton, W. J., & Zeigler, R. K. (1958). *Compressibility factors and fugacity coefficients calculated from the Beattie-Bridgeman equation of state for hydrogen, nitrogen, oxygen, carbon dioxide, ammonia, methane, and helium*. Los Alamos Scientific Lab., Los Alamos, NM (United States). Retrieved from https://www.osti.gov/servlets/purl/4289497

Huth, E., Muthu, S., Ruff, L., & Brant, J. A. (2014). Fbrineseasibility assessment of pervaporation for desalinating high-salinity brines. *Journal of Water Reuse and Desalination*, *4*(2), 109. https://doi.org/10.2166/wrd.2014.038

Ito, A., Feng, Y., & Sasaki, H. (1997). Temperature drop of feed liquid during pervaporation. *Journal of Membrane Science*, *133*, 95–102.

Jiang, J. S., Greenberg, D. B., & Fried, J. R. (1997). Pervaporation of methanol from a triglyme solution using a Nafion membrane: 2. Concentration polarization. *Journal of Membrane Science*, *132*(2), 263–271. https://doi.org/10.1016/S0376-7388(97)00066-5

Jyoti, G., Keshav, A., & Anandkumar, J. (2015). Review on Pervaporation : Theory , Membrane Performance , and Application to Intensification of Esterification Reaction. *Journal of Engineering*, *2015*.

Karlsson, H. O. E., & Trägårdh, G. (1996). Heat transfer in pervaporation. *Journal of Membrane Science*, *119*(2), 295–306. https://doi.org/10.1016/0376-7388(96)00150-0

Khayet, M., & Matsuura, T. (2004). Pervaporation and vacuum membrane distillation processes: Modeling and experiments. *AIChE Journal*, *50*(8), 1697–1712. https://doi.org/10.1002/aic.10161

Krishna, R., & Wesselingh, J. A. (1997). The Maxwell-Stefan approach to mass transfer. *Chemical Engineering Science*, *52*(6), 861–911.

Lawson, K. W., & Lloyd, D. R. (1997). Membrane distillation. *Journal of Membrane Science*, *124*(1), 1–25. https://doi.org/10.1016/S0376-7388(96)00236-0

Lide, D. R., Baysinger, G., Berger, L. I., Kehiaian, H. V, Roth, D. L., Zwillinger, D., … Haynes, W. M. (2009). CRC Handbook of Chemistry and Physics. *Group*. https://doi.org/10.1136/oem.53.7.504

Lipnizki, F., Hausmanns, S., & Field, R. W. (2004). Influence of impermeable components on the permeation of aqueous 1-propanol mixtures in hydrophobic pervaporation. *Journal of Membrane Science*, *228*, 129–138. https://doi.org/10.1016/j.memsci.2003.09.008

Lipnizki, F., Hausmanns, S., Ten, P., & Field, R. W. (1999). Organophilic pervaporation : prospects and performance. *Chemical Engineering Journal*, *73*, 113–129.

Magrí, A., Béline, F., & Dabert, P. (2013). Feasibility and interest of the anammox process as treatment alternative for anaerobic digester supernatants in manure processing - An overview. *Journal of Environmental Management*, *131*, 170–184. https://doi.org/10.1016/j.jenvman.2013.09.021

Martin, H. (2002). The generalized Lévêque equation and its practical use for the prediction of heat and mass transfer rates from pressure drop. *Chemical Engineering Science*, *57*(16), 3217–3223. https://doi.org/10.1016/S0009-2509(02)00194-X

Martínez-Díez, L., & Vázquez-González, M. . (1999). Temperature and concentration polarization in membrane distillation of aqueous salt solutions. *Journal of Membrane Science*, *156*(2), 265–273. https://doi.org/10.1016/S0376-7388(98)00349-4

Miessler, G. L., Fischer, P. J., & Tarr, D. A. (2014). *Inorganic Chemistry, 5th Edition*. PERSON. Retrieved from https://chemistlibrary.files.wordpress.com/2015/05/inorganic-chemistry-5th-edition-miessler.pdf

Moel, P. J. d, Verberk, J. Q. J. C., & Dijk, J. C. v. (2006). *Drinking Water: Principles And Practices*. World Scientific.

Munson, B. R., Okiishi, T. H., Rothmayer, A. P., & Huebsch, W. W. (2014). *Fundamentals of fluid mechanics*. John Wiley & Sons.

Nivaldo J, T. (2014). Chemistry_a_Molecular_Approach_Third_Edi.pdf.

Oliveira, T. A. C., Cocchini, U., Scarpello, J. T., & Livingston, A. G. (2001). Pervaporation mass transfer with liquid flow in the transition regime. *Journal of Membrane Science*, *183*(1), 119–133. https://doi.org/10.1016/S0376-7388(00)00576-7

Papadias, D. D., Ahmed, S., & Kumar, R. (2012). Fuel quality issues with biogas energy - An economic analysis for a stationary fuel cell system. *Energy*, *44*(1), 257–277. https://doi.org/10.1016/j.energy.2012.06.031

Park, H. B., Kamcev, J., Robeson, L. M., Elimelech, M., & Freeman, B. D. (2017). Maximizing the right stuff: The trade-off between membrane permeability and selectivity. *Science*, *356*(6343), 1138–1148. https://doi.org/10.1126/science.aab0530

Peng, M., Vane, L. M., & Liu, S. X. (2003). Recent advances in VOCs removal from water by pervaporation. *Journal of Hazardous Materials*, *98*(1–3), 69–90. https://doi.org/10.1016/S0304-3894(02)00360-6

Rautenbach, R., & Albrecht, R. (1980). Separation of organic binary mixture by pervaporation. *Journal of Mechanical Science and Technology*, *7*, 203–223.

Rosso, D., Larson, L. E., & Stenstrom, M. K. (2008). Aeration of large-scale municipal wastewater treatment plants: state of the art. *Water Science and Technology*, *57*(7), 973–978.

Shao, P., & Huang, R. Y. M. (2007). Polymeric membrane pervaporation. *Journal of Membrane Science*, *287*(2), 162–179. https://doi.org/10.1016/j.memsci.2006.10.043

Stambouli, A. B., & Traversa, E. (2002). Solid oxide fuel cells (SOFCs): A review of an environmentally clean and efficient source of energy. *Renewable and Sustainable Energy Reviews*, *6*(5), 433–455. https://doi.org/10.1016/S1364-0321(02)00014-X

Stumm, W., & Morgan, J. J. (2012). *Aquatic chemistry: chemical equilibria and rates in natural waters* (Vol. 126). John Wiley & Sons.

Thorndahl, U. (1993). Nitrogen Removal from Returned Liquors. *Water and Environment Journal*, *7*(5), 492–496. https://doi.org/10.1111/j.1747-6593.1993.tb00877.x

Trevani, L. N., Roberts, J. C., & Tremaine, P. R. (2001). Copper (II)–ammonia complexation equilibria in aqueous solutions at temperatures from 30 to 250° C by visible spectroscopy. *Journal of Solution Chemistry*, *30*(7), 585–622.

Uhlig, H. H. (1948). Corrosion handbook.

Valera-Medina, A., Xiao, H., Owen-Jones, M., David, W. I. F., & Bowen, P. J. (2018). Ammonia for power. *Progress in Energy and Combustion Science*, *69*, 63–102. https://doi.org/10.1016/J.PECS.2018.07.001

van Linden, N., Spanjers, H., & van Lier, J. (2016). *N2KWH: from pollutant to power*. *Poster session presented at PhD Energy Event, Delft, Netherlands.* Retrieved from https://pure.tudelft.nl/portal/files/16814492/Poster_Niels_van_Linden_N2kWh_Research_Final_30_Sep_16.pdf

Vane, L. M. (2005). A review of pervaporation for product recovery from biomass fermentation processes. *Journal of Chemical Technology and Biotechnology*, *80*(6), 603–629. https://doi.org/10.1002/jctb.1265

Wang, Q., Li, N., Bolto, B., Hoang, M., & Xie, Z. (2016). Desalination by pervaporation: A review. *Desalination*, *387*, 46–60. https://doi.org/10.1016/j.desal.2016.02.036

Wijmans, J. G., Athayde, A. L., Daniels, R., Ly, J. H., Kamaruddin, H. D., & Pinnau, I. (1996). The role of boundary layers in the removal of volatile organic compounds from water by pervaporation. *Journal of Membrane Science*, *109*(1), 135–146. https://doi.org/10.1016/0376-7388(95)00194-8

Wijmans, J. G., & Baker, R. W. (1995). The solution-diffusion model : a review. *Journal of Mechanical Science and Technology*, *107*, 1–21.

Yang, X., Ding, L., Wolf, M., Velterop, F., Bouwmeester, H. J. M., Smart, S., … Duke, M. (2016). Pervaporation of ammonia solution with γ-alumina supported organosilica membranes. *Separation and Purification Technology*, *168*, 141–151. https://doi.org/10.1016/j.seppur.2016.05.017

Yang, X., Fraser, T., Myat, D., Smart, S., Zhang, J., da Costa, J. C. D., … Duke, M. (2014). A pervaporation study of ammonia solutions using molecular sieve silica membranes. *Membranes*, *4*(1), 40–54. https://doi.org/10.3390/membranes4010040

Yang, X., Sheridan, S., Ding, L., Wang, D. K., Smart, S., Diniz da Costa, J. C., … Duke, M. (2018). Inter-layer free cobalt-doped silica membranes for pervaporation of ammonia solutions. *Journal of Membrane Science*, *553*(February), 111–116. https://doi.org/10.1016/j.memsci.2018.02.049

You, W.-T., Xu, Z.-L., Dong, Z.-Q., & Zhang, M. (2014). Vacuum membrane distillation–crystallization process

of high ammonium salt solutions. *Desalination and Water Treatment*, *55*(2), 368–380. https://doi.org/10.1080/19443994.2014.922499

Zhang, Y., Benes, N. E., & Lammertink, R. G. H. (2016). Performance study of pervaporation in a microfluidic system for the removal of acetone from water. *Chemical Engineering Journal*, *284*, 1342–1347. https://doi.org/10.1016/j.cej.2015.09.084

Appendix

Appendix A Total Flux

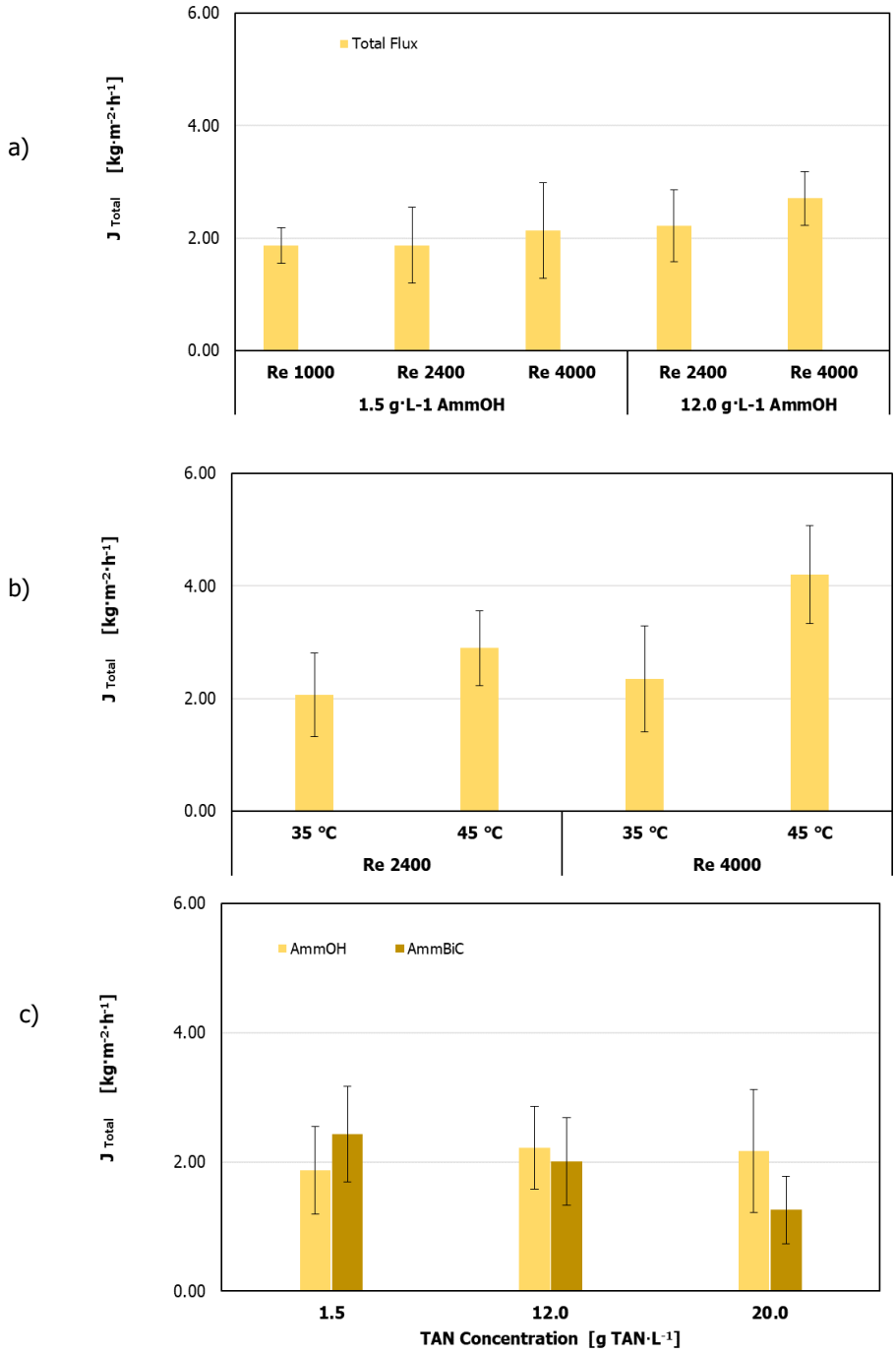

Figure 22 Total Flux of each experimental conditiona. a) Total flux over Reynodls number; b) Total flux over temperature;c) Total flux over Tan concentration and presence of additional salt. Error bars represent the standard deviation of samples taken in triplicate experiments.